

The PGPUC horizontal branch evolutionary tracks

Aldo A. R. Valcarce¹, Márcio Catelan^{2,3,4}, Sânia Alves¹, and Felipe González-Bordon¹

¹ Departamento de Física, FACI, Universidad de Tarapacá, Casilla 7D, Arica, Chile

² Instituto de Astrofísica, Pontifícia Universidad Católica de Chile, Av. Vicuña Mackenna 4860, 7820436 Macul, Santiago, Chile

³ Millennium Institute of Astrophysics, Nuncio Monseñor Sotero Sanz 100, Of. 104, Providencia, Santiago, Chile

⁴ Centro de Astro-Ingeniería, Pontifícia Universidad Católica de Chile, Av. Vicuña Mackenna 4860, 7820436 Macul, Santiago, Chile

Received XXXX XX, 2025; accepted XXXX XX, 202X

ABSTRACT

Context. The horizontal branch (HB) phase of stellar evolution plays a critical role in understanding the life cycle of stars, particularly in the context of low-mass stars. However, generating theoretical evolutionary tracks for HB stars is computationally intensive, especially when attempting to match a wide range of observational data.

Aims. This work presents an extensive grid of HB evolutionary tracks computed using the PGPUC code, covering a broad range of chemical compositions, progenitor masses, and alpha-element distributions. The aim is to provide a robust tool for interpreting HB stellar populations and advancing our understanding of their diverse properties. The evolutionary tracks are made publicly available through the PGPUC Online database for easy access and interpolation.

Methods. We computed over 19 000 HB evolutionary tracks encompassing a wide range in terms of mass, metallicity, helium abundance, and alpha-element enhancement, along with different progenitor masses. Using these tracks, we calculated zero-age, middle-age, and terminal-age loci.

Results. The PGPUC database now includes a fine grid of HB evolutionary tracks, allowing for precise interpolation. Key findings include the dependence of HB morphology on progenitor mass, metallicity, and helium abundance.

Key words. stars: abundances - stars: evolution - stars: horizontal branch

1. Introduction

The study of stellar evolution, particularly the horizontal branch (HB) phase, is crucial for understanding the life cycle of stars. The HB phase, characterized by helium core burning in low-to intermediate-mass stars, follows the red giant branch (RGB) phase and precedes the asymptotic giant branch (AGB) phase. This evolutionary stage is marked by a diverse range of stellar properties, influenced by initial chemical compositions and evolutionary histories, which makes it a key focus in astrophysical research (e.g., Salaris & Cassisi 2005; Catelan 2009).

In this sense, stellar evolutionary tracks are essential tools for interpreting observational data and understanding stellar populations. However, creating these tracks is computationally intensive and time-consuming, especially when a wide spectrum of initial parameters must be considered to match the observed diversity in stellar populations. Historically, researchers have dedicated significant resources to developing comprehensive sets of evolutionary tracks (e.g., Pietrinferni et al. 2004; Vandenberg et al. 2006; Dotter et al. 2008; Valcarce et al. 2012). These tracks typically vary in mass, global metallicity (Z), initial helium abundance (Y), and alpha-element enhancement ($[\alpha/\text{Fe}]$), reflecting the different chemical compositions observed in stars.

The progenitor mass (M_{MS}), defined here as the mass of the main sequence (MS) star that has just reached the RGB tip at a given age, is another critical parameter influencing the HB phase, particularly affecting the helium core mass (M_{cHe}). Understanding the impact of progenitor mass variations on HB stars is essential to accurately model their evolutionary paths and properties (Rood 1973). Despite the availability of various sets

of evolutionary tracks, the need for a rapidly accessible and comprehensive database of HB evolutionary tracks remains pressing.

In this paper, we present a new extensive set of HB evolutionary tracks computed using the Princeton-Goddard-Pontifícia Universidad Católica stellar evolution code (PGPUC SEC, Valcarce et al. 2012). This dataset includes over 19 000 evolutionary tracks with varying chemical compositions and progenitor masses, providing a robust tool for studying the effects of these parameters on HB stars. We have computed zero-age, middle-age, and terminal-age HB loci to investigate the impact of changing initial conditions on HB stellar populations. These evolutionary tracks are integrated into the PGPUC Online database, designed for fast interpolation and downloading, thereby facilitating efficient comparison of theoretical models with observational data.

This paper details the methodology used to generate the evolutionary tracks, the range of parameters considered, and a potential application. It is organized as follows. First, in Sect. 2 we describe the code used for creating the evolutionary tracks, followed by Sect. 3, which presents the HB evolutionary tracks created. Then, in Sect. 4 we describe the three main loci — zero-age, middle-age-, and terminal-age — that were created with these HB models, followed by the conclusions in Sect. 5.

2. The PGPUC stellar evolution code

The PGPUC SEC, described in full in Valcarce et al. (2012), represents an updated version of the code created by M. Schwarzschild and R. Härm at Princeton University (Schwarzschild & Härm 1965; Härm & Schwarzschild 1966), and then extensively modified by Allen V. Sweigart at NASA's

Goddard Space Flight Center (Sweigart 1971, 1973, 1994, 1997; Sweigart & Demarque 1972; Sweigart & Gross 1974, 1976; Sweigart & Catelan 1998, and references therein). The PGPUC SEC serves as a robust tool for primarily investigating low-mass stars spanning from the MS to the white dwarf cooling sequence. Low-mass stars are defined as those that develop a degenerate helium core following the MS evolution, corresponding to stars with masses below 2 or $3 M_{\odot}$, depending on their chemical composition.

2.1. Input physics

The physical inputs utilized in the PGPUC code include:

- Opacity for high temperatures in a tabular format from Iglesias & Rogers (1996) and for low temperatures from Ferguson et al. (2005);
- Conductive opacities from Cassisi et al. (2007);
- Neutrino energy losses based on the fitting formula by Haft et al. (1994);
- Thermonuclear reaction rates derived from the NACRE compilation (Angulo et al. 1999), with the exception of the $^{12}\text{C}(\alpha, \gamma)^{16}\text{O}$ reaction, which is sourced from Kunz et al. (2002);
- Irwin’s (2007) FreeEOS equation of state (EOS), option EOS4. The impact of this EOS on HB stellar models is discussed in Cassisi et al. (2003);
- Boundary conditions derived from Krishna Swamy (1966), fitted to a refined formula presented in Valcarce et al. (2012);
- Mass loss formula adapted from Schröder & Cuntz (2005) for the RGB phase (mass loss is turned off during the HB phase);
- Electron screening of nuclear reactions from DeWitt et al. (1973) and Grboske et al. (1973).¹

Proper treatment of semiconvection at the outer edge of the convective core is crucial to represent the HB phase correctly (Demarque & Mengel 1972). The PGPUC SEC treats this semiconvection with the procedure described in Sweigart & Demarque (1972). The treatment for suppressing the so-called breathing pulses is implemented as described in Sweigart (1971).

Horizontal branch models include an amount of extra helium in the envelope, typically $\Delta Y_{\text{RGB}} \leq 0.02$, depending on Z , Y , and M_{MS} (see Table B.1). This enrichment is associated with the occurrence of the first dredge-up during the RGB stage, which brings helium-rich material from the interior to the outer layers of the star (e.g., Iben 1964; Renzini 1977; Sweigart & Gross 1978).

Updates to some of these input physics ingredients have been provided in the literature in recent years. If taken into account, they would introduce small modifications to the resulting theoretical models and evolutionary tracks. In this work, we choose to maintain the original input physics (as in Valcarce et al. 2012) to ensure consistency with the existing PGPUC Online database. By keeping the same physical assumptions, we preserve the homogeneity between previously published PGPUC models and the new ones presented in this paper, ensuring that no discrepancies arise from differences in the input physics.

¹ Unlike what has been stated in some recent studies, PGPUC does not use electron screening from Salpeter (1954). Further details regarding this issue can be found in Appendix A.

2.2. The PGPUC Online database

The PGPUC Online database² enables users to interpolate evolutionary tracks from the MS to the tip of the RGB, isochrones, and zero-age horizontal branch (ZAHB) loci from a finely sampled grid of theoretical evolutionary tracks created utilizing the PGPUC SEC. Initially, this grid encompassed masses from $M = 0.5 M_{\odot}$ to $M = 1.1 M_{\odot}$, initial helium abundances from $Y = 0.230$ to $Y = 0.370$, and global metallicities from $Z = 0.00016$ to $Z = 0.01570$, with a fixed distribution of alpha-elements of $[\alpha/\text{Fe}] = \log(\alpha/\text{Fe}) - \log(\alpha/\text{Fe})_{\odot} = 0.3$ for a Grevesse & Sauval (1998) solar chemical composition, with our solar models being characterized by $(Z, Y)_{\odot} = (0.0167, 0.262)$ (Valcarce et al. 2012). Mass loss follows the Schröder & Cuntz (2005) prescription, with $\eta = 1.0$. Further details can be found in Valcarce et al. (2012). Over the past decade, this grid has been expanded to include models for $[\alpha/\text{Fe}] = 0.0$, and a mass loss rate with $\eta = 0.0$, as well as extending metallicities from $Z = 0.00001$ to $Z = 0.06000$ for evolutionary tracks and isochrones, and from $Z = 0.00001$ to $Z = 0.03000$ for ZAHB loci.

An essential input parameter for creating a ZAHB locus is M_{MS} , which, together with Z , Y , and $[\alpha/\text{Fe}]$, determines the M_{cHe} value at the tip of the RGB, and thus at the ZAHB. The M_{MS} parameter is particularly relevant for accurately predicting the position and shape of the ZAHB at high T_{eff} (e.g., $T_{\text{eff}} > 11\,500$ K) and defining the evolution throughout the HB phase (Eggleton 1968; Sweigart & Gross 1976, 1978; Vandenberg 1992). Higher values of this parameter ($M_{\text{MS}} > 1.0 M_{\odot}$) also influence the location of HB models at the red end. For a fixed chemical composition, HB models originating from higher M_{MS} progenitors tend to appear redder and more luminous than their lower-mass counterparts. This shift has important consequences for their pulsation properties (e.g., Cassisi et al. 1997).

The models provided by this database are available in the theoretical Hertzsprung–Russell diagram as well as in various photometric filters that can be chosen by the user. Currently, users have a choice from about 50 filter systems, primarily derived from bolometric corrections by Chen et al. (2019), as well as by Casagrande & Vandenberg (2018).

Moreover, this database includes two calculators for determining metallicity values and iron-over-hydrogen ratios ($[\text{Fe}/\text{H}]$). One calculator enables users to obtain the metallicity, Z , from a given $[\text{Fe}/\text{H}]$ value, helium mass fraction, Y , and alpha-element enhancement ratio, $[\alpha/\text{Fe}]$,³ while the other allows for the reverse calculation for obtaining $[\text{Fe}/\text{H}]$ from Z , Y , and $[\alpha/\text{Fe}]$.⁴ In the following section, we present a significant expansion of this grid to encompass the evolution of HB stars from the ZAHB to the terminal-age HB (TAHB).

3. Description of HB tracks

The HB evolutionary tracks (hereafter, the HB tracks) were calculated using the same grid of chemical compositions as the ones employed in the set of evolutionary tracks spanning from the MS to the tip of the RGB available in the PGPUC Online database. Specifically, this entails:

- Metallicity by mass: $Z = 0.00001, 0.00016, 0.00028, 0.00051, 0.00093, 0.00160, 0.00284, 0.00503, 0.00890, 0.01570$, and 0.03000 .

² <http://www2.astro.puc.cl/pgpuc/>

³ <http://www2.astro.puc.cl/pgpuc/Zcalculator.php>

⁴ <http://www2.astro.puc.cl/pgpuc/FeHcalculator.php>

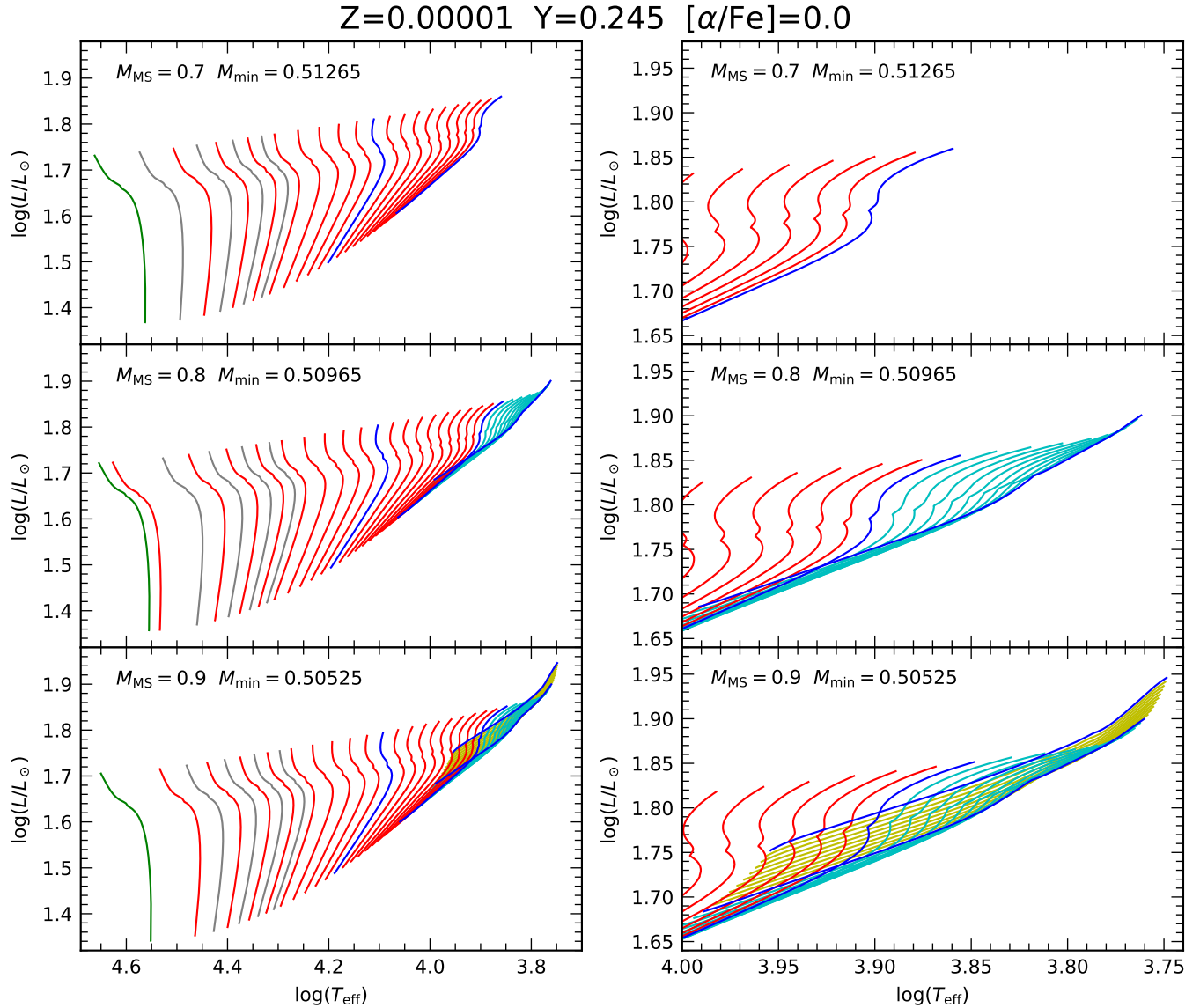


Fig. 1: HB evolutionary tracks in the theoretical plane — luminosity, $\log(L/L_\odot)$, vs. effective temperature, $\log T_{\text{eff}}$ — for $Z = 0.00001$, $Y = 0.245$, and $[\alpha/\text{Fe}] = 0.00$. The top, middle, and bottom left panels show the set of evolutionary tracks corresponding to progenitor masses of $M_{\text{MS}} = 0.700 M_\odot$, $0.800 M_\odot$, and $0.900 M_\odot$, respectively. The right panels are a zoom-in around the cooler part of the HB. Each panel also shows the minimum mass, M_{min} , reached for each set (green lines), corresponding to the hottest track. Blue, red, and gray lines correspond to evolutionary tracks in steps of $\Delta M = 0.100 M_\odot$, $\Delta M = 0.010 M_\odot$ (for masses lower than $0.700 M_\odot$), and $\Delta M = 0.005 M_\odot$ (for masses lower than $0.550 M_\odot$), respectively. Cyan lines correspond to evolutionary tracks computed with masses greater than $0.700 M_\odot$ and lower than $0.800 M_\odot$, in steps of $\Delta M = 0.010 M_\odot$. Yellow lines correspond to evolutionary tracks for masses greater than $0.800 M_\odot$ and lower than $0.900 M_\odot$, in steps of $\Delta M = 0.010 M_\odot$.

- Helium abundance by mass: $Y = 0.230, 0.245, 0.270, 0.295, 0.320, 0.345$, and 0.370 .
- Alpha-element enhancement ratio: $[\alpha/\text{Fe}] = 0.0$ and 0.3 .

We also included three different MS progenitor masses, namely $M_{\text{MS}} = 0.900$, 0.800 , and $0.700 M_\odot$, for each set of chemical compositions. This was done to account for the effect of age on a given stellar population, which is reflected in the initial M_{cHe} shared by all HB tracks for a given chemical composition and age. In this work, the evolution of the progenitor was computed from the MS to the ZAHB without mass loss. Thus, the maximum mass of a set of HB tracks is equal to the corresponding progenitor mass.

The masses used for the computations in a set of HB tracks (hereafter, M_{HB}) range from the mass of the progenitor down to $0.550 M_\odot$ in steps of $\Delta M = 0.010 M_\odot$, and from $0.550 M_\odot$ down to the lowest mass in each set (M_{min} , which differs from M_{cHe} by $\lesssim 0.0002 M_\odot$, in the sense that M_{cHe} is slightly smaller), in steps of $\Delta M = 0.005 M_\odot$. Note that the M_{min} value is different for different chemical compositions and M_{MS} values.

With all these variables considered, we computed a total of 19 441 HB tracks using the Geryon 2 supercomputer⁵, which amounted to a total of 1 620 days of CPU time. All these tracks

⁵ Geryon 2 is located at the Instituto de Astrofísica and managed in collaboration with the Centro de Astro-Ingeniería at Pontificia Universidad Católica de Chile.

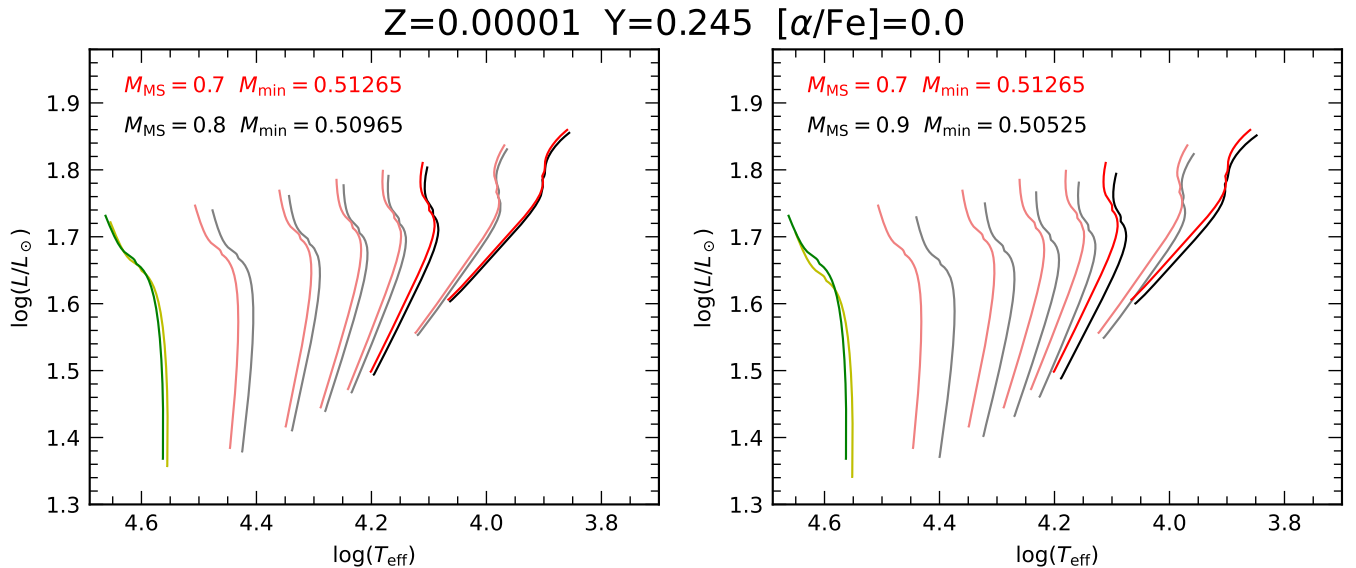


Fig. 2: Comparison between HB evolutionary tracks for $Z = 0.000010$, $Y = 0.245$, and $[\alpha/\text{Fe}] = 0.00$ with $M_{\text{MS}} = 0.700 M_{\odot}$ and: i) $M_{\text{MS}} = 0.800 M_{\odot}$ (left panel), and ii) $M_{\text{MS}} = 0.900 M_{\odot}$ (right panel). In each panel, green and yellow lines correspond to the M_{min} value reached for $M_{\text{MS}} = 0.700 M_{\odot}$ and the alternative M_{MS} value shown in the plot, respectively. Red and black lines correspond to masses in steps of $\Delta M = 0.010 M_{\odot}$ for $M_{\text{MS}} = 0.700 M_{\odot}$ and the alternative M_{MS} values, respectively. In like vein, red and gray lines correspond to evolutionary tracks for $M_{\text{MS}} = 0.700 M_{\odot}$ and the alternative M_{MS} values, respectively, with masses of $M_{\text{HB}} = 0.650 M_{\odot}, 0.580 M_{\odot}, 0.560 M_{\odot}, 0.540 M_{\odot}, 0.520 M_{\odot}$, and in steps of $\Delta M = 0.010 M_{\odot}$ for sets with evolutionary tracks that reach masses lower than $0.500 M_{\odot}$.

are included in the PGPUC Online database, providing a smooth grid for interpolating any parameter within the grid.

Figure 1 shows a set of computed HB tracks for $Z = 0.00001$, $[\alpha/\text{Fe}] = 0.0$, and $Y = 0.245$ and three M_{MS} values, demonstrating the smoothness of our grid. Figure 2 shows the comparison between HB tracks with $M_{\text{MS}} = 0.800$ and $0.900 M_{\odot}$ against $0.700 M_{\odot}$ for the same chemical composition as in Fig. 1.

The HB track with M_{min} is shown in each case; the models comprise a small H-rich envelope layer sitting on top of a core of initial mass M_{cHe} . The behavior of the HB tracks, including the loops observed at high metallicities and high helium abundances, closely aligns with that observed in other studies (e.g., Sweigart & Gross 1976; Bono et al. 1997b,a; Dotter et al. 2007; Pietrinferni et al. 2013). Similar figures, but for other chemical compositions, can be found in Appendix C.

Figure 2 reveals, as was expected, that the differences between the tracks computed for a fixed M_{HB} but different M_{MS} values increases as the difference in M_{MS} increases. This is particularly evident at lower M_{HB} values. This is due to the fact that, for larger M_{MS} values, the evolution progresses more rapidly along the RGB phase, resulting in a smaller M_{cHe} values (e.g., Sweigart & Gross 1978).

As was previously discussed by other authors (Faulkner 1966; Iben & Rood 1970; Gross 1973; Sweigart & Gross 1978; Dorman 1992, among others), the M_{cHe} value at the tip of the RGB is a physically well-defined quantity that depends sensitively on the progenitor's initial chemical composition and mass, as well as the adopted input physics. While earlier studies have typically reported M_{cHe} values for a limited set of input parameters, our updated PGPUC database provides this information systematically for a broad grid of compositions and M_{MS} . Table B.1 lists M_{cHe} , the age at the RGB tip, along with the associated helium enrichment in the envelope and both the ZAHB luminosity and mass at $\log T_{\text{eff}} = 3.83$ (a characteristic temperature of the

RR Lyrae instability strip) for each progenitor mass, M_{MS} , and chemical composition. These data show that M_{cHe} generally decreases with increasing Y and M_{MS} , with a lower variation when Z increases. This structured grid allows for a more continuous and accurate mapping of core masses across different stellar populations, and serves as a robust basis for the construction of HB models.

In order to facilitate the application of PGPUC models in stellar population studies, single HB tracks or complete sets of HB tracks covering the full mass range, from the selected M_{MS} to M_{min} , are available for bulk download from the HB section of the PGPUC Online webpage⁶. In order to avoid creating large files and make it easier to download the sets of HB tracks, the mass steps, ΔM_{HB} , were chosen as follows: $\Delta M_{\text{HB}} = 0.0100 M_{\odot}$ down to $M_{\text{HB}} = 0.550 M_{\odot}$, after which it decreases to $\Delta M_{\text{HB}} = 0.0050 M_{\odot}$ for lower masses. Sets of HB tracks with smaller mass steps can be requested via private communication.

Using these HB tracks, it is also possible to calculate the ZAHB, middle-age horizontal branch (MAHB), and TAHB loci for any given chemical composition, which can also be downloaded from the PGPUC Online database. These loci are described in detail in the following section.

4. ZAHB, MAHB, and TAHB loci

To facilitate comparisons between observations and theory, we have used HB tracks to define, as we have done in previous studies (Catelan et al. 2009; Valcarce et al. 2014, 2016), three key reference loci – ZAHB, MAHB, and TAHB – each corresponding to a different evolutionary moment in the HB phase. In particular, in addition to the ZAHB, we used two main percentage time loci, following their original definitions given in Catelan et al. (2009):

⁶ <http://www2.astro.puc.cl/pgpuc/hb.php>

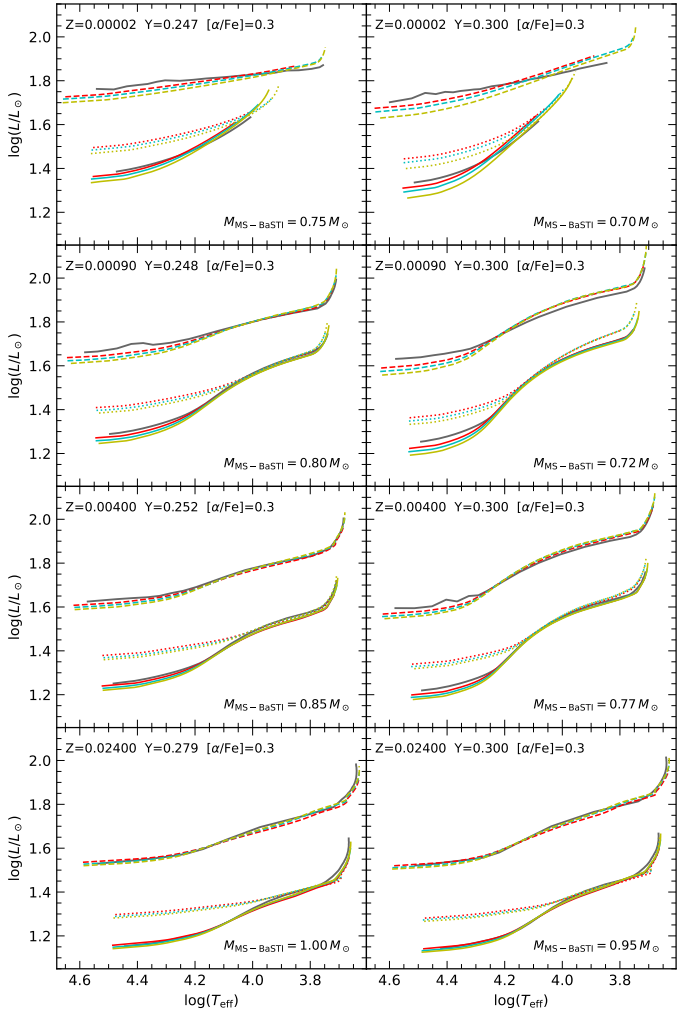


Fig. 3: PGPUC ZAHB (continuous lines), MAHB (dotted lines), and TAHB loci (dashed lines) in the theoretical plane for eight chemical compositions listed in each panel. Red, cyan, and yellow lines correspond to progenitor masses of 0.700, 0.800, and 0.900 M_{\odot} , respectively. In gray are shown ZAHB and TAHB loci from BaSTI for comparison, with the progenitor mass of those models indicated in each panel.

- TAHB loci, corresponding, for a given chemical composition and M_{MS} value, to the geometrical locus connecting HB stars with different ZAHB masses in the luminosity (absolute magnitude) versus effective temperature (color) plane when the He at their cores is depleted;
- MAHB loci, which are analogous to the TAHB loci, except that they are computed at the halfway point (in terms of age) of the entire HB evolutionary phase.

It is important to note that the MAHB loci correspond to different absolute ages for each HB mass at any given chemical composition, since HB stars with lower masses evolve more slowly than their more massive counterparts (Sweigart & Gross 1976; Castellani et al. 1994; Zoccali et al. 2000). Examples of these loci are presented in Fig. 3 within the theoretical ($\log L$, $\log T_{\text{eff}}$) plane, showing a diverse set of chemical compositions. The dependence of the ZAHB, MAHB, and TAHB loci on different M_{MS} values is clearly observed. Here, it is possible to observe that the luminosity difference between the ZAHB and MAHB is larger at high T_{eff} . The luminosity difference between

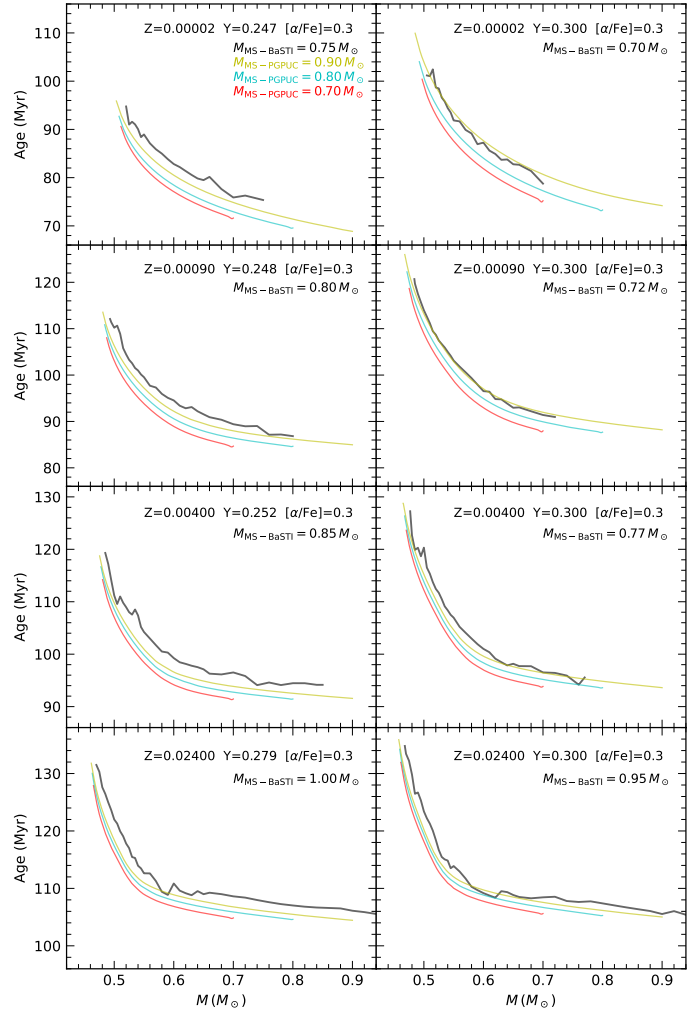


Fig. 4: TAHB age values for HB stars as a function of the HB mass. Red, cyan, and yellow lines correspond to progenitor masses of 0.700, 0.800, and 0.900 M_{\odot} , respectively, while in gray are shown BaSTI TAHB loci for comparison, with the progenitor mass of the BaSTI models indicated in each panel.

the ZAHB and MAHB is most pronounced at high T_{eff} , while at intermediate T_{eff} this difference becomes almost negligible. The specific T_{eff} at which this transition occurs depends on the chemical composition.

At the low T_{eff} end (corresponding to high M_{HB}), the separation between these loci re-emerges, becoming more evident at higher Y . These findings emphasize the importance of carefully selecting the appropriate metallicity and helium abundance when comparing these evolutionary lines against observations. Interpolation of the HB tracks within a finely sampled grid is therefore crucial to avoid misrepresenting the theoretical results.

Figure 3 also includes a comparison with “a Bag of Stellar Tracks and Isochrones” (BaSTI) models with $[\alpha/\text{Fe}] = 0.4$ (Hidalgo et al. 2018; Pietrinferni et al. 2021), demonstrating that their ZAHB and TAHB loci (for the available M_{MS}) share similar properties to the ones from the PGPUC models. The primary differences occur at high temperatures, where the PGPUC models extend to higher T_{eff} and lower M_{HB} . Additionally, at the lowest metallicities, the PGPUC models exhibit small differences in luminosity ($\Delta \log[L/L_{\odot}] \approx 0.01$) compared to the BaSTI models for canonical He abundances, increasing to $\Delta \log(L/L_{\odot}) \approx 0.03$

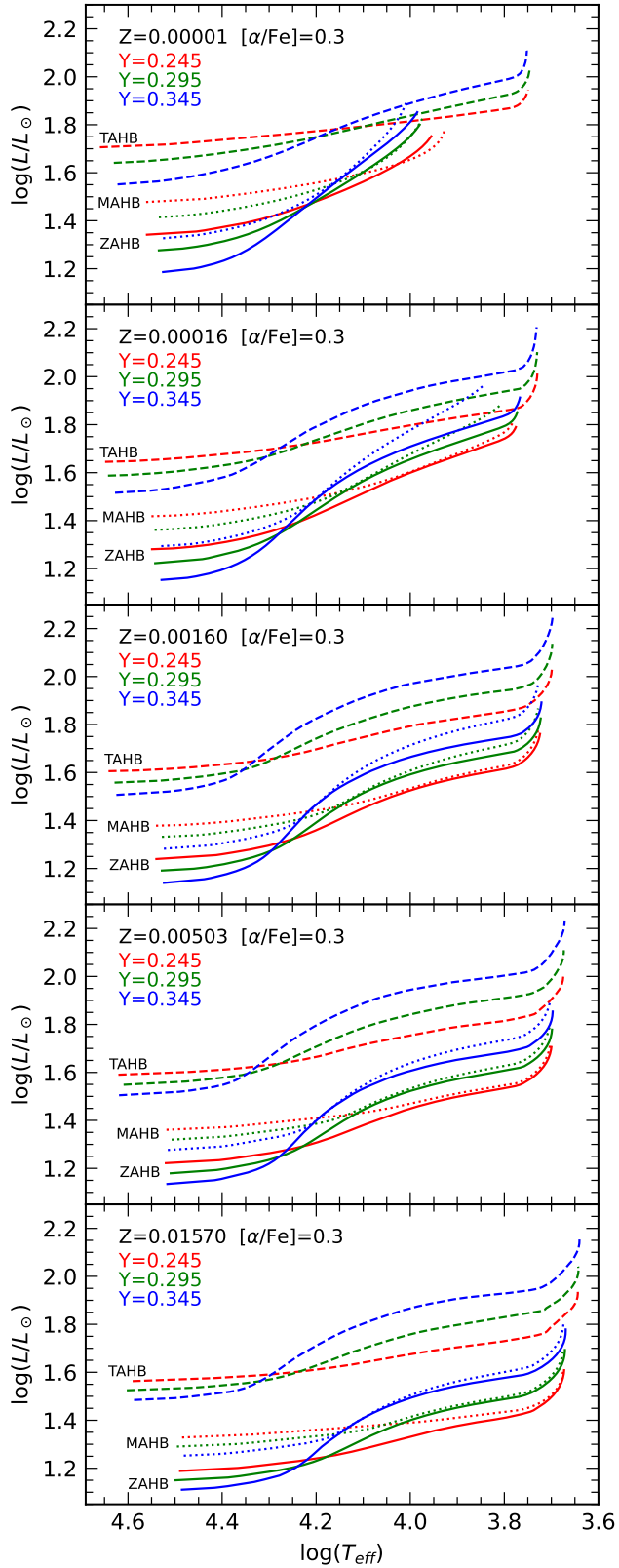


Fig. 5: ZAHB (continuous lines), MAHB (dotted lines), and TAHB loci in the theoretical plane for five metallicities, increasing from the top to the bottom panels, for $M_{\text{MS}} = 0.900 M_\odot$ and $[\alpha/\text{Fe}] = 0.3$. Red, green, and blue lines correspond to helium abundances of $Y = 0.245$, 0.295 , and 0.345 , respectively.

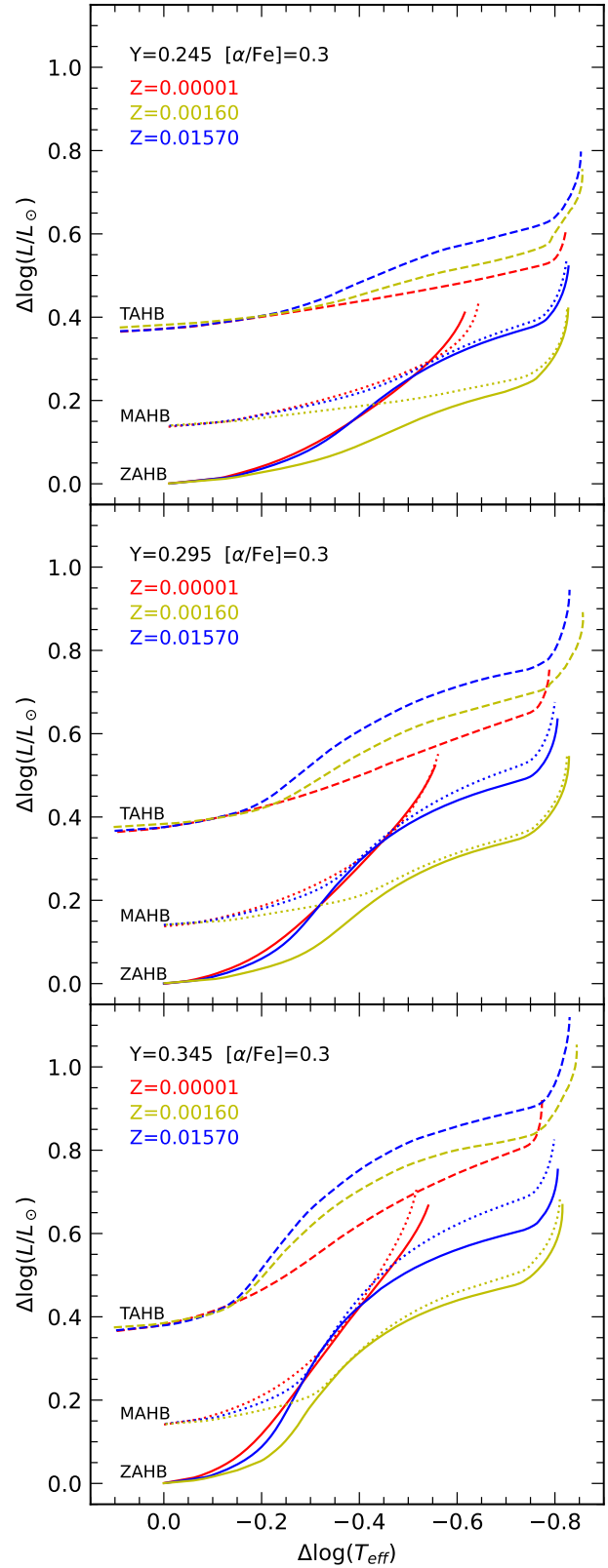


Fig. 6: Comparison of ZAHB (continuous lines), MAHB (dotted lines), and TAHB loci in the theoretical plane for three metallicities ($Z = 0.00001$, 0.00160 and 0.01570 in red, yellow, and blue, respectively) and three helium abundances ($Y = 0.245$, 0.295 , and 0.345 in the top, middle, and bottom panels, respectively). In all displayed cases, $M_{\text{MS}} = 0.900 M_\odot$ and $[\alpha/\text{Fe}] = 0.3$ have been assumed. All models have been shifted in $\log(L/L_\odot)$ and $\log T_{\text{eff}}$ such that the highest T_{eff} of each ZAHB locus aligns at the origin.

for He-rich models. Those differences decrease when the metallicity increases. Regarding the evolutionary timescales from the ZAHB to the TAHB, Fig. 4 presents the corresponding lifetimes for the same models shown in Fig. 3. When compared to the BaSTI models, the differences are typically $\lesssim 10$ Myr across the full mass range. These discrepancies may arise from differences in the adopted input physics and/or the assumed solar heavy-element mixture.

The effects of the Z value on the ZAHB locus have been well documented in the literature (Faulkner & Iben 1966; Iben & Faulkner 1968; Iben & Rood 1970; Sweigart 1987; Caputo & Degl'Innocenti 1995; Valcarce et al. 2012, among others); however, this is not the case for MAHB and TAHB loci. Figures 5 and 6 show that the TAHB T_{eff} extension is rather stable as a function of chemical composition, with the main noteworthy trend being an overall shift to higher temperatures with increasing Z . The ZAHB and MAHB loci, on the other hand, are much less extended in T_{eff} . This is due, on the one hand, to the fact that ZAHB and MAHB loci never reach temperatures in excess of $\log T_{\text{eff}} \approx 4.55$, which, however, are easily surpassed at the TAHB level. On the other, at the very lowest metallicities, ZAHB models never reach temperatures low enough as to reach the red HB or even the instability strip region (whose temperature range is about $6000 \text{ K} \lesssim T_{\text{eff}} \lesssim 7250 \text{ K}$; Catelan & Smith 2015). This is consistent with the trend (also observed in, for instance, Sweigart 1987; VandenBerg 2024) of increasing minimum ZAHB temperature with decreasing metallicity. These trends imply that, at sufficiently low metallicities, the only red HB or RR Lyrae stars that can exist are those that are close to exhausting He in their cores. Extremely metal-poor ($Z \lesssim 0.0001$) red HB stars and RR Lyrae should thus be very rare. This conclusion, originally investigated from a theoretical perspective by Cassisi et al. (1996, 1997), is consistent with the recent analysis of three extremely metal-poor RR Lyrae stars by D’Orazi et al. (2025).

Another interesting effect seen in Fig. 5 that involves ZAHB and MAHB loci is that, for some chemical compositions, these loci share the same $\log(L/L_{\odot})$ value at a given $\log(T_{\text{eff}})$. In some cases, the MAHB locus even becomes fainter than the ZAHB locus. This is due to the fact that, at a given T_{eff} , depending on the chemical composition, the MAHB level of an HB track may be less luminous than the ZAHB level of another HB track. Indeed, it is worth noting that, for some chemical compositions, the blue loops developed by some evolutionary tracks may reach luminosities that are lower than the ZAHB. This effect can also be seen in the HB tracks presented by Sweigart (1987).

For low Y , the crossing point between the ZAHB and MAHB moves to lower T_{eff} as Z increases, while when Y increases, this point moves to higher T_{eff} as Z increases. For T_{eff} values lower than the crossing point, ZAHB and MAHB loci have different behaviors depending on Y and Z . At low Y , ZAHB and MAHB loci share similar $\log(T_{\text{eff}})$ and $\log(L/L_{\odot})$ values at high Z , but at very low metallicities, the MAHB locus can be fainter than the ZAHB locus. When Y increases, there is a notable increase in the difference in $\log(L/L_{\odot})$ between ZAHB and MAHB, causing HB stars to be spread over a larger space in the $(\log L, \log T_{\text{eff}})$ plane. For T_{eff} values higher than the crossing point, there is a gradual increase in the difference in $\log(L/L_{\odot})$ between ZAHB and MAHB that is less affected by Z and Y than happens at T_{eff} values lower than the crossing point.

As to the impact of differences in M_{MS} , the most significant differences in ZAHB, MAHB, and TAHB loci, as is observed in Fig. 3, are seen primarily at higher temperatures, where a higher M_{MS} value results in a lower luminosity at a given T_{eff} . This phenomenon is particularly pronounced at low Z and high Y .

The effect is produced by the larger spread in M_{cHe} values when varying M_{MS} at the metal-poor and He-rich end (see Table B.1).

Even though the ZAHB, MAHB, and TAHB loci show similar shapes in the $(\log L, \log T_{\text{eff}})$ plane when changing M_{MS} for some chemical compositions, the M_{HB} value at a given T_{eff} does change when M_{MS} changes. In this sense, one must be very careful when masses of HB stars are obtained from these loci without considering the most appropriate M_{MS} value for a given age. Differences can reach as much as 6 000 K at low M_{HB} values (i.e., at the hot end of the HB) for high Z and low Y ; more generally, the range in T_{eff} values increases for lower Z and higher Y . Although these considerations must be kept in mind when comparing observational data to theoretical models, present-day observational uncertainties in hot HB stars’ T_{eff} values (e.g., Latour et al. 2023) are of the same order of magnitude as the differences in T_{eff} predicted by assuming different M_{MS} values.

5. Summary and conclusions

This work introduces an extensive set of HB tracks computed with the PGPUC code. Spanning over 19,000 evolutionary tracks, this dataset accounts for a broad range of chemical compositions and progenitor masses, providing a comprehensive resource for the study of HB stars. Integrated into the PGPUC Online database, these HB tracks enable fast interpolation and an efficient comparison with observational data.

The PGPUC Online database now offers precise interpolation capabilities from the ZAHB to the TAHB, including HB tracks for different progenitor masses. This capability is critical for interpreting high-accuracy present-day observational data and serves as a very useful tool for examining the evolutionary phases of HB stars.

Our results highlight the dependency of HB stellar properties on initial conditions, such as Z , Y , and M_{MS} . In particular:

- The M_{min} value decreases with increasing Z and Y , with higher M_{MS} leading to lower M_{min} .
- At high Z , the M_{min} value is nearly constant for any M_{MS} or Y values. However, at low Z , the difference in the M_{min} value when varying M_{MS} becomes more pronounced as Y increases.

The morphology of HB loci in the theoretical plane is strongly influenced by initial parameters. Notably, higher M_{MS} values result in lower luminosities at a given effective temperature, emphasizing the importance of the progenitor’s mass (hence age) in modeling the evolution of HB stars.

In conclusion, the expanded PGPUC Online database provides a robust framework for investigating HB stellar populations. By incorporating a wide array of initial parameters and offering publicly accessible tools for interpolation, this unique resource can be leveraged to address outstanding questions about HB morphology, the formation of blue and extreme HB stars, and how the latter are affected by changes in chemical composition and age.

Acknowledgements. We thank the referee, S. Cassisi, for a helpful report. We also thank Yang Chen for his valuable assistance with the implementation of the PARSEC bolometric corrections into the PGPUC Online database. Support for this project is provided by ANID’s FONDECYT Regular grants #1171273 and #1231637; ANID’s Millennium Science Initiative through grants ICN12_009 and AIM23-0001, awarded to the Millennium Institute of Astrophysics (MAS); and ANID’s Basal project FB210003. The Geryon cluster at the Centro de Astro-Ingeniería UC was extensively used for the calculations performed in this paper. BASAL CATA PFB-06, the Anillo ACT-86, FONDEQUIP AIC-57, and QUIMAL 130008 provided funding for several improvements to the Geryon cluster.

References

- Angulo, C., Arnould, M., Rayet, M., et al. 1999, Nucl. Phys. A, 656, 3
 Bono, G., Caputo, F., Cassisi, S., Castellani, V., & Marconi, M. 1997a, ApJ, 489, 822
 Bono, G., Caputo, F., Cassisi, S., Castellani, V., & Marconi, M. 1997b, ApJ, 479, 279
 Caputo, A. & Raffelt, G. 2024, in 1st General Meeting and 1st Training School of the COST Action COSMIC WISPerS, Vol. 1, 41
 Caputo, F. & Degl'Innocenti, S. 1995, A&A, 298, 833
 Carenza, P., Giannotti, M., Isern, J., Mirizzi, A., & Straniero, O. 2025, Phys. Rep., 1117, 1
 Casagrande, L. & Vandenberg, D. A. 2018, MNRAS, 475, 5023
 Cassisi, S., Castellani, M., & Castellani, V. 1997, A&A, 317, 108
 Cassisi, S., Castellani, V., & Tornambe, A. 1996, ApJ, 459, 298
 Cassisi, S., Potekhin, A. Y., Pietrinferni, A., Catelan, M., & Salaris, M. 2007, ApJ, 661, 1094
 Cassisi, S., Salaris, M., & Irwin, A. W. 2003, ApJ, 588, 862
 Castellani, M., Castellani, V., Pulone, L., & Tornambe, A. 1994, A&A, 282, 771
 Catelan, M. 2009, Ap&SS, 320, 261
 Catelan, M., Grundahl, F., Sweigart, A. V., Valcarce, A. A. R., & Cortés, C. 2009, ApJ, 695, L97
 Catelan, M. & Smith, H. A. 2015, Pulsating Stars (Wiley-VCH, Weinheim)
 Chen, Y., Girardi, L., Fu, X., et al. 2019, A&A, 632, A105
 Demarque, P. & Mengel, J. G. 1972, ApJ, 171, 583
 DeWitt, H. E., Graboske, H. C., & Cooper, M. S. 1973, ApJ, 181, 439
 D'Orazi, V., Braga, V., Bono, G., et al. 2025, A&A, 694, A158
 Dorman, B. 1992, ApJS, 80, 701
 Dotter, A., Chaboyer, B., Jevremović, D., et al. 2007, AJ, 134, 376
 Dotter, A., Chaboyer, B., Jevremović, D., et al. 2008, ApJS, 178, 89
 Eggleton, P. P. 1968, MNRAS, 140, 387
 Faulkner, J. 1966, ApJ, 144, 978
 Faulkner, J. & Iben, Jr., I. 1966, ApJ, 144, 995
 Ferguson, J. W., Alexander, D. R., Allard, F., et al. 2005, ApJ, 623, 585
 Graboske, H. C., Dewitt, H. E., Grossman, A. S., & Cooper, M. S. 1973, ApJ, 181, 457
 Grevesse, N. & Sauval, A. J. 1998, Space Sci. Rev., 85, 161
 Gross, P. G. 1973, MNRAS, 164, 65
 Haft, M., Raffelt, G., & Weiss, A. 1994, ApJ, 425, 222
 Härm, R. & Schwarzschild, M. 1966, ApJ, 145, 496
 Hidalgo, S. L., Pietrinferni, A., Cassisi, S., et al. 2018, ApJ, 856, 125
 Iben, Jr., I. 1964, ApJ, 140, 1631
 Iben, Jr., I. & Faulkner, J. 1968, ApJ, 153, 101
 Iben, Jr., I. & Rood, R. T. 1970, ApJ, 161, 587
 Iglesias, C. A. & Rogers, F. J. 1996, ApJ, 464, 943
 Irwin, A. W. 2007, <http://freeeos.sourceforge.net>
 Krishna Swamy, K. S. 1966, ApJ, 145, 174
 Kunz, R., Fey, M., Jaeger, M., et al. 2002, ApJ, 567, 643
 Latour, M., Hämerich, S., Dorsch, M., et al. 2023, A&A, 677, A86
 Pietrinferni, A., Cassisi, S., Salaris, M., & Castelli, F. 2004, ApJ, 612, 168
 Pietrinferni, A., Cassisi, S., Salaris, M., & Hidalgo, S. 2013, A&A, 558, A46
 Pietrinferni, A., Hidalgo, S., Cassisi, S., et al. 2021, ApJ, 908, 102
 Renzini, A. 1977, in Saas-Fee Advanced Course 7: Advanced Stages in Stellar Evolution, ed. P. Bouvier & A. Maeder, 151
 Rood, R. T. 1973, ApJ, 184, 815
 Salaris, M. & Cassisi, S. 2005, Evolution of Stars and Stellar Populations
 Salpeter, E. E. 1954, Australian Journal of Physics, 7, 373
 Schröder, K. P. & Cuntz, M. 2005, ApJ, 630, L73
 Schwarzschild, M. & Härm, R. 1965, ApJ, 142, 855
 Serenelli, A., Weiss, A., Cassisi, S., Salaris, M., & Pietrinferni, A. 2017, A&A, 606, A33
 Straniero, O., Pallanca, C., Dalessandro, E., et al. 2020, A&A, 644, A166
 Sweigart, A. V. 1971, ApJ, 168, 79
 Sweigart, A. V. 1973, A&A, 24, 459
 Sweigart, A. V. 1987, ApJS, 65, 95
 Sweigart, A. V. 1994, ApJ, 426, 612
 Sweigart, A. V. 1997, ApJ, 474, L23
 Sweigart, A. V. & Catelan, M. 1998, ApJ, 501, L63
 Sweigart, A. V. & Demarque, P. 1972, A&A, 20, 445
 Sweigart, A. V. & Gross, P. G. 1974, ApJ, 190, 101
 Sweigart, A. V. & Gross, P. G. 1976, ApJS, 32, 367
 Sweigart, A. V. & Gross, P. G. 1978, ApJS, 36, 405
 Valcarce, A. A. R. 2011, Study of the Helium Enrichment in Globular Clusters (Ph.D. Thesis, Pontificia Universidad Católica de Chile)
 Valcarce, A. A. R., Catelan, M., Alonso-García, J., Contreras Ramos, R., & Alves, S. 2016, A&A, 589, A126
 Valcarce, A. A. R., Catelan, M., Alonso-García, J., Cortés, C., & De Medeiros, J. R. 2014, ApJ, 782, 85
 Valcarce, A. A. R., Catelan, M., & Sweigart, A. V. 2012, A&A, 547, A5
 Vandenberg, D. A. 1992, ApJ, 391, 685
 Vandenberg, D. A. 2024, MNRAS, 527, 6888
 Vandenberg, D. A., Bergbusch, P. A., & Dowler, P. D. 2006, ApJS, 162, 375
 Vandenberg, D. A., Swenson, F. J., Rogers, F. J., Iglesias, C. A., & Alexander, D. R. 2000, ApJ, 532, 430
 Viaux, N., Catelan, M., Stetson, P. B., et al. 2013a, Phys. Rev. Lett., 111, 231301
 Viaux, N., Catelan, M., Stetson, P. B., et al. 2013b, A&A, 558, A12
 Zoccali, M., Cassisi, S., Bono, G., et al. 2000, ApJ, 538, 289

Appendix A: Electron screening and the RGB tip luminosity

Valcarce et al. (2012) carried out a comparison between the results obtained with PGPUC and five other SECs. PGPUC's predecessor, the Princeton-Goddard (PG) SEC (see their Sect. 2 for extensive references), was also added to that analysis. One noteworthy result of these comparisons, well illustrated in their Fig. 3, is the realization that, for similar input parameters, there is a fairly wide range in predicted RGB tip luminosities. In particular, PG and PGPUC predict the faintest RGB tips. A comparison between PG and Victoria results had previously been carried out by VandenBerg et al. (2000), who found that PG predicted similar but slightly fainter RGB tips and ZAHB loci, in spite of very similar M_{cHe} values.

The reason why this happens is unclear, and explaining it is well beyond the scope of the present paper. However, it has been suggested in the literature (Serenelli et al. 2017; Straniero et al. 2020; Caputo & Raffelt 2024; Carenza et al. 2025) that this can be traced in part to the fact that PGPUC presumably uses Salpeter's formulation of weak screening of nuclear reactions (Salpeter 1954), leading to inaccurate predictions of the position of the RGB tip luminosity, as compared to other codes that use more up-to-date recipes for electron screening.

This explanation is not correct. As explained in Sweigart & Gross (1978, Sect. II.b), the DeWitt et al. (1973) and Grboske et al. (1973) prescriptions were adopted early on in the development of the PG code to account for electron screening. PGPUC is an updated version of the PG SEC (Valcarce et al. 2012). While the input physics in PGPUC has been extensively updated since Sweigart & Gross (1978), it still relies, as do other state-of-the-art SECs, on DeWitt et al. (1973) and Grboske et al. (1973) for the treatment of electron screening.

The confusion appears to stem from a misinterpretation of Viaux et al. (2013a,b), where PGPUC models were used to carry out a detailed study of the RGB tip position in the GC M5 (NGC 5904). As the only reference that Viaux et al. cite to introduce the subject of screening is Salpeter (1954), this may have led to the incorrect impression that Salpeter's prescriptions were used in the actual calculations, when in fact they were not. The fact that electron screening is not specifically addressed in either Valcarce (2011) or Valcarce et al. (2012) may have contributed to the confusion.

In conclusion, whatever the ultimate explanation for the differences in RGB tip position between PG/PGPUC and other codes, they are most certainly not due to adoption of the Salpeter (1954) prescription for electron screening of nuclear reactions in either PG or PGPUC. A deeper analysis will be required to fully understand the reason why different SECs still predict significantly different RGB tip luminosities.

Appendix B: Supplementary table

Table B.1 lists key physical properties of stellar models at the RGB tip and near the RR Lyrae instability strip. For each combination of chemical composition (\bar{Y} , Z) and progenitor mass M_{MS} , we report the helium core mass at the RGB tip (M_{cHe}), the amount of additional helium in the envelope due to the first dredge-up (ΔY_{RGB}), the stellar age at the RGB tip (from the zero-age MS), and the luminosity ($\log L_{3.83}^{\text{RRL}}$) and stellar mass ($M_{3.83}^{\text{RRL}}$) of the ZAHB model with $\log T_{\text{eff}} = 3.83$ (which is a common reference temperature near the center of the RR Lyrae instability strip). For each Z value, solar-scaled and α -enhanced compositions are considered ($[\alpha/\text{Fe}] = 0.0$ and 0.3 , respectively). At very low metallicities, ZAHB models may not reach this temperature, in which case the corresponding $\log L_{3.83}^{\text{RRL}}$ and $M_{3.83}^{\text{RRL}}$ values are not provided. $[\text{Fe}/\text{H}]$ values are calculated assuming $Y = 0.245$.

Table B.1: Stellar model parameters for different Z , Y , and M_{MS} values.

Y	M_{MS}	M_{cHe}	ΔY_{RGB}	Age	$\log L_{3.83}^{\text{RRL}}$	$M_{3.83}^{\text{RRL}}$	Y	M_{MS}	M_{cHe}	ΔY_{RGB}	Age	$\log L_{3.83}^{\text{RRL}}$	$M_{3.83}^{\text{RRL}}$
$Z = 0.00001$													
[Fe/H] = -3.24, [α/Fe] = 0.00							[Fe/H] = -3.47, [α/Fe] = 0.30						
0.230	0.700	0.5165	0.0002	21866	—	—	0.230	0.700	0.5167	0.0002	21867	—	—
	0.800	0.5138	0.0025	13587	—	—		0.800	0.5140	0.0025	13589	—	—
	0.900	0.5099	0.0066	9005	—	—		0.900	0.5101	0.0065	9007	—	—
0.245	0.700	0.5126	0.0003	19989	—	—	0.245	0.700	0.5128	0.0003	19990	—	—
	0.800	0.5096	0.0028	12428	—	—		0.800	0.5098	0.0028	12430	—	—
	0.900	0.5052	0.0068	8246	—	—		0.900	0.5054	0.0067	8248	—	—
0.270	0.700	0.5060	0.0005	17162	—	—	0.270	0.700	0.5062	0.0005	17164	—	—
	0.800	0.5023	0.0032	10686	—	—		0.800	0.5025	0.0031	10688	—	—
	0.900	0.4969	0.0070	7107	—	—		0.900	0.4971	0.0069	7109	—	—
0.295	0.700	0.4992	0.0007	14685	—	—	0.295	0.700	0.4994	0.0007	14686	—	—
	0.800	0.4946	0.0035	9162	—	—		0.800	0.4948	0.0035	9163	—	—
	0.900	0.4879	0.0070	6109	—	—		0.900	0.4880	0.0070	6110	—	—
0.320	0.700	0.4921	0.0009	12523	—	—	0.320	0.700	0.4922	0.0009	12524	—	—
	0.800	0.4865	0.0038	7833	—	—		0.800	0.4867	0.0037	7833	—	—
	0.900	0.4775	0.0069	5236	—	—		0.900	0.4776	0.0068	5236	—	—
0.345	0.700	0.4846	0.0012	10619	—	—	0.345	0.700	0.4848	0.0011	10644	—	—
	0.800	0.4775	0.0039	6658	—	—		0.800	0.4778	0.0039	6677	—	—
	0.900	0.4655	0.0068	4474	—	—		0.900	0.4657	0.0067	4474	—	—
0.370	0.700	0.4767	0.0014	9017	—	—	0.370	0.700	0.4769	0.0013	9017	—	—
	0.800	0.4678	0.0040	5673	—	—		0.800	0.4679	0.0039	5673	—	—
	0.900	0.4516	0.0065	3800	—	—		0.900	0.4519	0.0065	3805	—	—
$Z = 0.00016$													
[Fe/H] = -2.04, [α/Fe] = 0.00							[Fe/H] = -2.26, [α/Fe] = 0.30						
0.230	0.700	0.5004	0.0017	22090	—	—	0.230	0.700	0.5007	0.0017	22102	—	—
	0.800	0.4970	0.0066	13698	1.699	0.783		0.800	0.4973	0.0064	13705	1.703	0.790
	0.900	0.4933	0.0116	9052	1.697	0.776		0.900	0.4935	0.0114	9055	1.701	0.784
0.245	0.700	0.4967	0.0020	20185	—	—	0.245	0.700	0.4970	0.0019	20195	—	—
	0.800	0.4932	0.0069	12521	1.718	0.783		0.800	0.4934	0.0067	12526	1.722	0.790
	0.900	0.4891	0.0116	8286	1.714	0.775		0.900	0.4893	0.0114	8286	1.718	0.783
0.270	0.700	0.4905	0.0025	17318	—	—	0.270	0.700	0.4907	0.0024	17326	—	—
	0.800	0.4865	0.0073	10754	1.749	0.780		0.800	0.4867	0.0071	10757	1.753	0.788
	0.900	0.4820	0.0114	7130	1.741	0.770		0.900	0.4821	0.0112	7132	1.746	0.778
0.295	0.700	0.4841	0.0030	14805	—	—	0.295	0.700	0.4844	0.0029	14810	—	—
	0.800	0.4797	0.0074	9209	1.778	0.774		0.800	0.4799	0.0073	9211	1.783	0.782
	0.900	0.4745	0.0111	6122	1.768	0.761		0.900	0.4746	0.0110	6121	1.772	0.769
0.320	0.700	0.4775	0.0034	12614	—	—	0.320	0.700	0.4777	0.0032	12616	—	—
	0.800	0.4725	0.0074	7864	1.807	0.765		0.800	0.4727	0.0073	7864	1.811	0.772
	0.900	0.4665	0.0107	5241	1.792	0.749		0.900	0.4665	0.0106	5240	1.796	0.756
0.345	0.700	0.4708	0.0037	10710	—	—	0.345	0.700	0.4710	0.0036	10710	—	—
	0.800	0.4651	0.0073	6695	1.834	0.752		0.800	0.4652	0.0072	6694	1.838	0.760
	0.900	0.4579	0.0102	4473	1.813	0.732		0.900	0.4578	0.0100	4472	1.817	0.739
0.370	0.700	0.4639	0.0039	9062	—	—	0.370	0.700	0.4640	0.0038	9061	—	—
	0.800	0.4572	0.0070	5682	1.859	0.737		0.800	0.4573	0.0070	5681	1.864	0.744
	0.900	0.4484	0.0095	3806	1.832	0.714		0.900	0.4483	0.0095	3804	1.835	0.720
$Z = 0.00028$													
[Fe/H] = -1.79, [α/Fe] = 0.00							[Fe/H] = -2.02, [α/Fe] = 0.30						
0.230	0.700	0.4973	0.0024	22384	—	—	0.230	0.700	0.4975	0.0023	22395	—	—
	0.800	0.4939	0.0078	13873	1.669	0.730		0.800	0.4941	0.0075	13878	1.673	0.736
	0.900	0.4903	0.0128	9156	1.667	0.725		0.900	0.4905	0.0125	9158	1.670	0.731
0.245	0.700	0.4937	0.0027	20449	—	—	0.245	0.700	0.4939	0.0026	20457	—	—
	0.800	0.4901	0.0080	12676	1.687	0.728		0.800	0.4903	0.0078	12680	1.691	0.735
	0.900	0.4863	0.0127	8376	1.684	0.722		0.900	0.4865	0.0125	8377	1.688	0.729
0.270	0.700	0.4875	0.0032	17538	—	—	0.270	0.700	0.4878	0.0031	17543	—	—
	0.800	0.4837	0.0083	10881	1.717	0.723		0.800	0.4839	0.0081	10883	1.721	0.730
	0.900	0.4795	0.0125	7205	1.711	0.716		0.900	0.4796	0.0123	7204	1.715	0.722
0.295	0.700	0.4813	0.0038	14988	—	—	0.295	0.700	0.4815	0.0036	14991	—	—
	0.800	0.4772	0.0085	9313	1.747	0.717		0.800	0.4773	0.0083	9313	1.751	0.723
	0.900	0.4724	0.0121	6181	1.738	0.707		0.900	0.4724	0.0119	6180	1.742	0.713

Continued on next page

Table B.1: Continued.

Y	M_{MS}	M_{cHe}	ΔY_{RGB}	Age	$\log L_{3.83}^{\text{RRL}}$	$M_{3.83}^{\text{RRL}}$	Y	M_{MS}	M_{cHe}	ΔY_{RGB}	Age	$\log L_{3.83}^{\text{RRL}}$	$M_{3.83}^{\text{RRL}}$
	(M_{\odot})	(M_{\odot})		(Myr)		(M_{\odot})		(M_{\odot})	(M_{\odot})		(Myr)		(M_{\odot})
0.320	0.700	0.4750	0.0042	12764	—	—	0.320	0.700	0.4752	0.0041	12763	—	—
	0.800	0.4703	0.0084	7946	1.776	0.707		0.800	0.4704	0.0082	7945	1.780	0.714
	0.900	0.4649	0.0116	5288	1.765	0.696		0.900	0.4649	0.0114	5286	1.768	0.702
0.345	0.700	0.4685	0.0045	10833	—	—	0.345	0.700	0.4686	0.0044	10826	—	—
	0.800	0.4632	0.0082	6761	1.805	0.696		0.800	0.4633	0.0081	6758	1.809	0.702
	0.900	0.4570	0.0110	4511	1.790	0.684		0.900	0.4569	0.0108	4508	1.793	0.688
0.370	0.700	0.4618	0.0046	9160	1.849	0.698	0.370	0.700	0.4619	0.0045	9155	—	—
	0.800	0.4558	0.0079	5734	1.833	0.684		0.800	0.4558	0.0077	5730	1.840	0.688
	0.900	0.4484	0.0103	3837	1.813	0.669		0.900	0.4483	0.0102	3833	1.815	0.673
$Z = 0.00051$													
[Fe/H] = -1.53, [α/Fe] = 0.00							[Fe/H] = -1.76, [α/Fe] = 0.30						
0.230	0.700	0.4941	0.0031	22978	1.639	0.690	0.230	0.700	0.4943	0.0030	22981	1.643	0.696
	0.800	0.4908	0.0091	14229	1.640	0.686		0.800	0.4910	0.0088	14225	1.644	0.692
	0.900	0.4875	0.0142	9375	1.639	0.682		0.900	0.4876	0.0140	9367	1.643	0.688
0.245	0.700	0.4906	0.0036	20983	1.658	0.688	0.245	0.700	0.4908	0.0034	20983	1.662	0.694
	0.800	0.4871	0.0093	12997	1.658	0.684		0.800	0.4873	0.0091	12991	1.662	0.689
	0.900	0.4837	0.0140	8571	1.656	0.679		0.900	0.4838	0.0138	8562	1.660	0.684
0.270	0.700	0.4846	0.0041	17985	1.690	0.683	0.270	0.700	0.4849	0.0040	17981	1.695	0.689
	0.800	0.4810	0.0096	11145	1.689	0.678		0.800	0.4811	0.0094	11137	1.693	0.683
	0.900	0.4772	0.0137	7365	1.684	0.672		0.900	0.4773	0.0135	7355	1.689	0.678
0.295	0.700	0.4786	0.0047	15360	1.723	0.677	0.295	0.700	0.4787	0.0045	15353	1.727	0.682
	0.800	0.4747	0.0096	9529	1.720	0.671		0.800	0.4748	0.0094	9519	1.724	0.676
	0.900	0.4706	0.0132	6312	1.713	0.664		0.900	0.4705	0.0130	6302	1.717	0.669
0.320	0.700	0.4725	0.0052	13070	1.756	0.669	0.320	0.700	0.4726	0.0050	13061	1.760	0.674
	0.800	0.4683	0.0095	8122	1.751	0.662		0.800	0.4683	0.0093	8112	1.755	0.667
	0.900	0.4637	0.0126	5394	1.742	0.654		0.900	0.4635	0.0124	5384	1.745	0.659
0.345	0.700	0.4663	0.0055	11081	1.789	0.660	0.345	0.700	0.4663	0.0053	11069	1.794	0.665
	0.800	0.4616	0.0092	6903	1.782	0.652		0.800	0.4616	0.0091	6891	1.786	0.657
	0.900	0.4564	0.0119	4597	1.770	0.643		0.900	0.4562	0.0117	4587	1.773	0.648
0.370	0.700	0.4599	0.0056	9361	1.824	0.651	0.370	0.700	0.4599	0.0054	9349	1.828	0.656
	0.800	0.4547	0.0088	5848	1.812	0.642		0.800	0.4546	0.0087	5837	1.816	0.646
	0.900	0.4488	0.0111	3906	1.797	0.631		0.900	0.4484	0.0109	3896	1.799	0.635
$Z = 0.00093$													
[Fe/H] = -1.27, [α/Fe] = 0.00							[Fe/H] = -1.50, [α/Fe] = 0.30						
0.230	0.700	0.4911	0.0040	24044	1.609	0.654	0.230	0.700	0.4913	0.0039	24037	1.614	0.659
	0.800	0.4880	0.0104	14877	1.610	0.651		0.800	0.4881	0.0101	14863	1.615	0.656
	0.900	0.4849	0.0154	9780	1.610	0.647		0.900	0.4850	0.0152	9761	1.614	0.653
0.245	0.700	0.4877	0.0045	21942	1.628	0.651	0.245	0.700	0.4878	0.0043	21935	1.633	0.656
	0.800	0.4845	0.0106	13578	1.629	0.648		0.800	0.4846	0.0103	13562	1.633	0.653
	0.900	0.4814	0.0154	8931	1.628	0.644		0.900	0.4814	0.0150	8914	1.632	0.649
0.270	0.700	0.4819	0.0052	18789	1.661	0.646	0.270	0.700	0.4821	0.0049	18779	1.666	0.651
	0.800	0.4786	0.0108	11627	1.661	0.642		0.800	0.4786	0.0105	11611	1.666	0.647
	0.900	0.4753	0.0149	7662	1.658	0.638		0.900	0.4753	0.0146	7645	1.662	0.643
0.295	0.700	0.4761	0.0058	16029	1.695	0.640	0.295	0.700	0.4762	0.0056	16016	1.700	0.644
	0.800	0.4727	0.0108	9926	1.693	0.635		0.800	0.4726	0.0106	9908	1.698	0.640
	0.900	0.4692	0.0144	6556	1.689	0.630		0.900	0.4690	0.0141	6538	1.693	0.635
0.320	0.700	0.4703	0.0062	13623	1.730	0.633	0.320	0.700	0.4703	0.0060	13608	1.735	0.637
	0.800	0.4666	0.0107	8447	1.726	0.628		0.800	0.4665	0.0104	8428	1.731	0.632
	0.900	0.4628	0.0137	5594	1.720	0.622		0.900	0.4626	0.0135	5576	1.724	0.626
0.345	0.700	0.4644	0.0065	11535	1.765	0.624	0.345	0.700	0.4644	0.0063	11518	1.770	0.629
	0.800	0.4604	0.0103	7167	1.760	0.619		0.800	0.4602	0.0101	7148	1.764	0.623
	0.900	0.4561	0.0128	4760	1.750	0.612		0.900	0.4558	0.0126	4743	1.754	0.616
0.370	0.700	0.4584	0.0066	9731	1.801	0.616	0.370	0.700	0.4583	0.0064	9711	1.806	0.620
	0.800	0.4539	0.0098	6063	1.793	0.609		0.800	0.4538	0.0096	6043	1.797	0.613
	0.900	0.4493	0.0120	4039	1.781	0.602		0.900	0.4492	0.0117	4022	1.785	0.606
$Z = 0.00160$													
[Fe/H] = -1.04, [α/Fe] = 0.00							[Fe/H] = -1.26, [α/Fe] = 0.30						
0.230	0.700	0.4886	0.0048	25702	1.578	0.627	0.230	0.700	0.4887	0.0046	25695	1.583	0.632
	0.800	0.4857	0.0114	15895	1.580	0.624		0.800	0.4857	0.0112	15865	1.584	0.630
	0.900	0.4829	0.0166	10425	1.581	0.622		0.900	0.4829	0.0163	10389	1.585	0.626

Continued on next page

Table B.1: Continued.

Y	M_{MS}	M_{cHe}	ΔY_{RGB}	Age	$\log L_{3.83}^{\text{RRL}}$	$M_{3.83}^{\text{RRL}}$	Y	M_{MS}	M_{cHe}	ΔY_{RGB}	Age	$\log L_{3.83}^{\text{RRL}}$	$M_{3.83}^{\text{RRL}}$		
	(M_{\odot})	(M_{\odot})		(Myr)		(M_{\odot})		(M_{\odot})	(M_{\odot})		(Myr)		(M_{\odot})		
0.245	0.700	0.4853	0.0053	23443	1.598	0.624	0.245	0.700	0.4854	0.0050	23428	1.603	0.629		
	0.800	0.4823	0.0117	14493	1.600	0.621		0.800	0.4825	0.0114	14462	1.605	0.627		
	0.900	0.4795	0.0164	9510	1.599	0.618		0.900	0.4795	0.0162	9473	1.604	0.623		
0.270	0.700	0.4798	0.0061	20051	1.632	0.619	0.270	0.700	0.4798	0.0059	20028	1.638	0.623		
	0.800	0.4767	0.0119	12393	1.633	0.615		0.800	0.4767	0.0116	12358	1.638	0.620		
	0.900	0.4738	0.0160	8141	1.631	0.612		0.900	0.4737	0.0157	8105	1.636	0.617		
0.295	0.700	0.4742	0.0068	17086	1.668	0.613	0.295	0.700	0.4742	0.0065	17057	1.673	0.617		
	0.800	0.4710	0.0119	10561	1.667	0.609		0.800	0.4709	0.0116	10524	1.672	0.613		
	0.900	0.4680	0.0154	6950	1.664	0.605		0.900	0.4678	0.0151	6915	1.668	0.610		
0.320	0.700	0.4686	0.0072	14504	1.705	0.606	0.320	0.700	0.4686	0.0069	14469	1.711	0.610		
	0.800	0.4653	0.0117	8970	1.702	0.602		0.800	0.4651	0.0114	8932	1.707	0.606		
	0.900	0.4620	0.0145	5918	1.697	0.598		0.900	0.4618	0.0144	5884	1.702	0.602		
0.345	0.700	0.4630	0.0074	12263	1.742	0.599	0.345	0.700	0.4629	0.0072	12225	1.748	0.603		
	0.800	0.4594	0.0112	7595	1.737	0.594		0.800	0.4593	0.0110	7557	1.743	0.598		
	0.900	0.4560	0.0137	5025	1.731	0.590		0.900	0.4557	0.0135	4993	1.735	0.593		
0.370	0.700	0.4573	0.0075	10328	1.781	0.591	0.370	0.700	0.4572	0.0072	10287	1.786	0.595		
	0.800	0.4535	0.0107	6411	1.773	0.586		0.800	0.4533	0.0105	6374	1.779	0.590		
	0.900	0.4498	0.0127	4255	1.765	0.581		0.900	0.4494	0.0125	4225	1.769	0.584		
$Z = 0.00284$															
	[Fe/H] = -0.79, [α/Fe] = 0.00								[Fe/H] = -1.01, [α/Fe] = 0.30						
0.230	0.700	0.4862	0.0055	28644	1.540	0.603	0.230	0.700	0.4863	0.0052	28618	1.544	0.607		
	0.800	0.4836	0.0125	17704	1.543	0.601		0.800	0.4836	0.0122	17652	1.547	0.606		
	0.900	0.4812	0.0176	11584	1.544	0.599		0.900	0.4811	0.0174	11523	1.549	0.604		
0.245	0.700	0.4831	0.0060	26099	1.560	0.601	0.245	0.700	0.4831	0.0058	26061	1.565	0.605		
	0.800	0.4804	0.0128	16126	1.563	0.598		0.800	0.4803	0.0124	16068	1.568	0.603		
	0.900	0.4778	0.0175	10549	1.563	0.595		0.900	0.4779	0.0173	10488	1.569	0.601		
0.270	0.700	0.4778	0.0069	22289	1.596	0.595	0.270	0.700	0.4778	0.0066	22234	1.602	0.600		
	0.800	0.4750	0.0129	13761	1.598	0.593		0.800	0.4750	0.0127	13696	1.603	0.597		
	0.900	0.4726	0.0170	9004	1.598	0.591		0.900	0.4724	0.0167	8941	1.602	0.595		
0.295	0.700	0.4724	0.0075	18962	1.634	0.590	0.295	0.700	0.4724	0.0074	18895	1.640	0.594		
	0.800	0.4696	0.0128	11699	1.633	0.587		0.800	0.4695	0.0126	11631	1.640	0.591		
	0.900	0.4671	0.0163	7662	1.632	0.584		0.900	0.4669	0.0161	7600	1.637	0.588		
0.320	0.700	0.4671	0.0081	16068	1.673	0.584	0.320	0.700	0.4670	0.0078	15995	1.679	0.587		
	0.800	0.4642	0.0125	9911	1.671	0.581		0.800	0.4641	0.0123	9841	1.677	0.584		
	0.900	0.4617	0.0155	6502	1.667	0.577		0.900	0.4613	0.0153	6443	1.673	0.581		
0.345	0.700	0.4618	0.0083	13559	1.712	0.577	0.345	0.700	0.4616	0.0081	13482	1.719	0.580		
	0.800	0.4588	0.0121	8366	1.709	0.574		0.800	0.4586	0.0120	8298	1.715	0.577		
	0.900	0.4560	0.0144	5503	1.704	0.570		0.900	0.4556	0.0143	5447	1.709	0.574		
0.370	0.700	0.4564	0.0084	11393	1.753	0.570	0.370	0.700	0.4562	0.0082	11315	1.760	0.573		
	0.800	0.4532	0.0115	7039	1.747	0.566		0.800	0.4530	0.0114	6973	1.754	0.570		
	0.900	0.4503	0.0133	4644	1.743	0.563		0.900	0.4499	0.0133	4592	1.747	0.565		
$Z = 0.00503$															
	[Fe/H] = -0.54, [α/Fe] = 0.00								[Fe/H] = -0.76, [α/Fe] = 0.30						
0.230	0.700	0.4839	0.0059	33629	1.493	0.583	0.230	0.700	0.4839	0.0057	33567	1.497	0.587		
	0.800	0.4814	0.0132	20761	1.497	0.581		0.800	0.4814	0.0130	20669	1.501	0.585		
	0.900	0.4793	0.0185	13556	1.498	0.579		0.900	0.4792	0.0183	13458	1.503	0.584		
0.245	0.700	0.4807	0.0070	30609	1.514	0.580	0.245	0.700	0.4808	0.0063	30518	1.518	0.585		
	0.800	0.4784	0.0134	18886	1.516	0.578		0.800	0.4783	0.0133	18786	1.522	0.583		
	0.900	0.4762	0.0184	12324	1.517	0.577		0.900	0.4761	0.0181	12223	1.524	0.581		
0.270	0.700	0.4757	0.0075	26067	1.550	0.576	0.270	0.700	0.4757	0.0073	25965	1.557	0.580		
	0.800	0.4733	0.0138	16081	1.554	0.574		0.800	0.4732	0.0135	15970	1.559	0.578		
	0.900	0.4712	0.0179	10484	1.554	0.572		0.900	0.4710	0.0176	10380	1.558	0.576		
0.295	0.700	0.4707	0.0083	22128	1.591	0.571	0.295	0.700	0.4706	0.0081	22011	1.597	0.575		
	0.800	0.4682	0.0137	13637	1.591	0.568		0.800	0.4681	0.0135	13521	1.599	0.573		
	0.900	0.4660	0.0171	8888	1.590	0.566		0.900	0.4658	0.0169	8785	1.597	0.570		
0.320	0.700	0.4656	0.0089	18706	1.632	0.565	0.320	0.700	0.4655	0.0087	18583	1.639	0.568		
	0.800	0.4631	0.0135	11517	1.632	0.563		0.800	0.4629	0.0133	11401	1.638	0.566		
	0.900	0.4609	0.0163	7510	1.629	0.560		0.900	0.4606	0.0161	7412	1.635	0.564		
0.345	0.700	0.4605	0.0092	15747	1.673	0.559	0.345	0.700	0.4604	0.0090	15619	1.682	0.562		
	0.800	0.4580	0.0130	9687	1.671	0.556		0.800	0.4577	0.0129	9575	1.679	0.560		
	0.900	0.4558	0.0153	6327	1.668	0.554		0.900	0.4554	0.0151	6234	1.674	0.557		
0.370	0.700	0.4555	0.0092	13197	1.717	0.553	0.370	0.700	0.4553	0.0090	13070	1.725	0.555		

Continued on next page

Table B.1: Continued.

Y	M_{MS} (M_{\odot})	M_{cHe} (M_{\odot})	ΔY_{RGB}	Age (Myr)	$\log L_{3.83}^{\text{RRL}}$	$M_{3.83}^{\text{RRL}}$ (M_{\odot})	Y	M_{MS} (M_{\odot})	M_{cHe} (M_{\odot})	ΔY_{RGB}	Age (Myr)	$\log L_{3.83}^{\text{RRL}}$	$M_{3.83}^{\text{RRL}}$ (M_{\odot})
	0.800	0.4528	0.0124	8117	1.714	0.550		0.800	0.4526	0.0122	8010	1.722	0.553
	0.900	0.4506	0.0141	5315	1.709	0.547		0.900	0.4502	0.0140	5230	1.717	0.550
$Z = 0.00890$													
[Fe/H] = -0.29, [α/Fe] = 0.00							[Fe/H] = -0.51, [α/Fe] = 0.30						
0.230	0.700	0.4810	0.0061	41905	1.433	0.564	0.230	0.700	0.4812	0.0058	41781	1.439	0.569
	0.800	0.4789	0.0138	25811	1.439	0.563		0.800	0.4788	0.0135	25647	1.443	0.567
	0.900	0.4770	0.0192	16827	1.442	0.561		0.900	0.4769	0.0190	16662	1.446	0.566
0.245	0.700	0.4783	0.0069	38038	1.455	0.563	0.245	0.700	0.4783	0.0066	37899	1.459	0.567
	0.800	0.4760	0.0142	23433	1.459	0.561		0.800	0.4760	0.0140	23264	1.465	0.565
	0.900	0.4741	0.0190	15269	1.461	0.559		0.900	0.4740	0.0190	15102	1.468	0.564
0.270	0.700	0.4734	0.0079	32285	1.492	0.559	0.270	0.700	0.4734	0.0078	32124	1.500	0.563
	0.800	0.4712	0.0145	19889	1.496	0.556		0.800	0.4711	0.0143	19712	1.504	0.561
	0.900	0.4693	0.0187	12945	1.497	0.555		0.900	0.4691	0.0185	12777	1.504	0.560
0.295	0.700	0.4686	0.0088	27307	1.534	0.554	0.295	0.700	0.4685	0.0086	27127	1.541	0.558
	0.800	0.4664	0.0145	16818	1.537	0.552		0.800	0.4662	0.0144	16636	1.543	0.556
	0.900	0.4645	0.0179	10930	1.537	0.551		0.900	0.4643	0.0178	10767	1.544	0.554
0.320	0.700	0.4637	0.0095	23014	1.578	0.549	0.320	0.700	0.4636	0.0093	22821	1.587	0.553
	0.800	0.4615	0.0142	14160	1.579	0.547		0.800	0.4614	0.0141	13979	1.588	0.551
	0.900	0.4597	0.0170	9193	1.577	0.545		0.900	0.4594	0.0169	9035	1.585	0.549
0.345	0.700	0.4589	0.0099	19318	1.623	0.543	0.345	0.700	0.4588	0.0096	19118	1.633	0.547
	0.800	0.4567	0.0138	11872	1.622	0.541		0.800	0.4565	0.0136	11693	1.631	0.545
	0.900	0.4548	0.0159	7704	1.619	0.539		0.900	0.4545	0.0159	7555	1.628	0.543
0.370	0.700	0.4542	0.0100	16145	1.677	0.537	0.370	0.700	0.4540	0.0098	15944	1.680	0.541
	0.800	0.4519	0.0132	9908	1.668	0.535		0.800	0.4517	0.0131	9735	1.678	0.538
	0.900	0.4500	0.0147	6436	1.664	0.533		0.900	0.4497	0.0148	6296	1.674	0.536
$Z = 0.01570$													
[Fe/H] = -0.04, [α/Fe] = 0.00							[Fe/H] = -0.26, [α/Fe] = 0.30						
0.230	0.700	0.4776	0.0060	55021	1.366	0.546	0.230	0.700	0.4776	0.0059	54953	1.373	0.551
	0.800	0.4754	0.0142	33842	1.371	0.545		0.800	0.4755	0.0140	33651	1.378	0.550
	0.900	0.4736	0.0201	22014	1.374	0.544		0.900	0.4736	0.0199	21790	1.381	0.549
0.245	0.700	0.4748	0.0069	49854	1.385	0.545	0.245	0.700	0.4748	0.0067	49739	1.391	0.550
	0.800	0.4727	0.0147	30643	1.390	0.544		0.800	0.4727	0.0144	30437	1.396	0.548
	0.900	0.4709	0.0199	19933	1.393	0.543		0.900	0.4709	0.0199	19702	1.400	0.547
0.270	0.700	0.4701	0.0082	42141	1.421	0.542	0.270	0.700	0.4702	0.0080	41969	1.429	0.547
	0.800	0.4681	0.0151	25900	1.428	0.541		0.800	0.4680	0.0150	25670	1.436	0.545
	0.900	0.4663	0.0195	16840	1.429	0.539		0.900	0.4663	0.0195	16604	1.438	0.544
0.295	0.700	0.4655	0.0092	35491	1.464	0.538	0.295	0.700	0.4655	0.0091	35273	1.473	0.543
	0.800	0.4635	0.0153	21812	1.468	0.537		0.800	0.4634	0.0152	21570	1.477	0.541
	0.900	0.4618	0.0188	14169	1.469	0.535		0.900	0.4617	0.0188	13933	1.478	0.540
0.320	0.700	0.4609	0.0100	29775	1.509	0.534	0.320	0.700	0.4609	0.0099	29529	1.520	0.538
	0.800	0.4589	0.0150	18302	1.514	0.533		0.800	0.4588	0.0150	18049	1.522	0.536
	0.900	0.4574	0.0178	11872	1.512	0.531		0.900	0.4571	0.0179	11640	1.522	0.535
0.345	0.700	0.4564	0.0105	24886	1.558	0.529	0.345	0.700	0.4563	0.0104	24621	1.570	0.532
	0.800	0.4545	0.0146	15292	1.558	0.527		0.800	0.4542	0.0146	15036	1.570	0.531
	0.900	0.4528	0.0167	9904	1.555	0.525		0.900	0.4526	0.0168	9679	1.568	0.529
0.370	0.700	0.4519	0.0107	20718	1.608	0.524	0.370	0.700	0.4517	0.0106	20440	1.619	0.527
	0.800	0.4499	0.0140	12718	1.607	0.522		0.800	0.4496	0.0139	12466	1.620	0.525
	0.900	0.4482	0.0155	8227	1.607	0.520		0.900	0.4480	0.0156	8014	1.620	0.523
$Z = 0.03000$													
[Fe/H] = 0.25, [α/Fe] = 0.00							[Fe/H] = 0.03, [α/Fe] = 0.30						
0.230	0.700	0.4711	0.0064	77421	1.279	0.526	0.230	0.700	0.4712	0.0062	77230	1.295	0.529
	0.800	0.4691	0.0148	48185	1.283	0.525		0.800	0.4692	0.0147	47811	1.298	0.528
	0.900	0.4674	0.0212	31263	1.285	0.524		0.900	0.4675	0.0212	30872	1.300	0.527
0.245	0.700	0.4686	0.0073	70264	1.295	0.525	0.245	0.700	0.4685	0.0072	69990	1.309	0.528
	0.800	0.4664	0.0154	43501	1.299	0.524		0.800	0.4665	0.0153	43103	1.313	0.527
	0.900	0.4649	0.0210	28201	1.301	0.523		0.900	0.4649	0.0211	27807	1.317	0.526
0.270	0.700	0.4641	0.0086	59395	1.327	0.523	0.270	0.700	0.4641	0.0086	59027	1.343	0.526
	0.800	0.4621	0.0161	36550	1.333	0.522		0.800	0.4621	0.0161	36130	1.349	0.525
	0.900	0.4606	0.0206	23680	1.336	0.521		0.900	0.4606	0.0207	23286	1.352	0.524
0.295	0.700	0.4597	0.0099	49854	1.370	0.520	0.295	0.700	0.4597	0.0099	49430	1.386	0.523

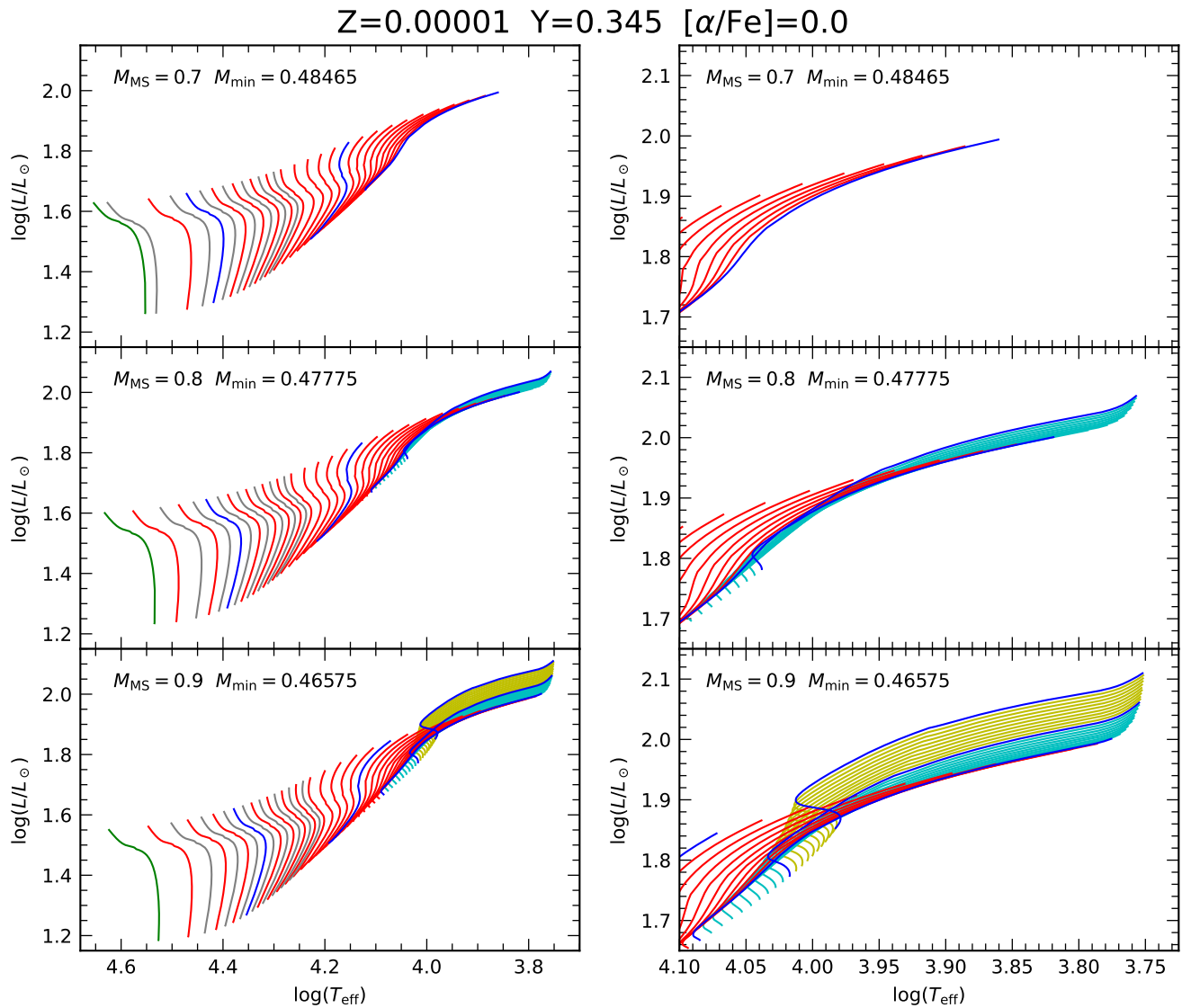
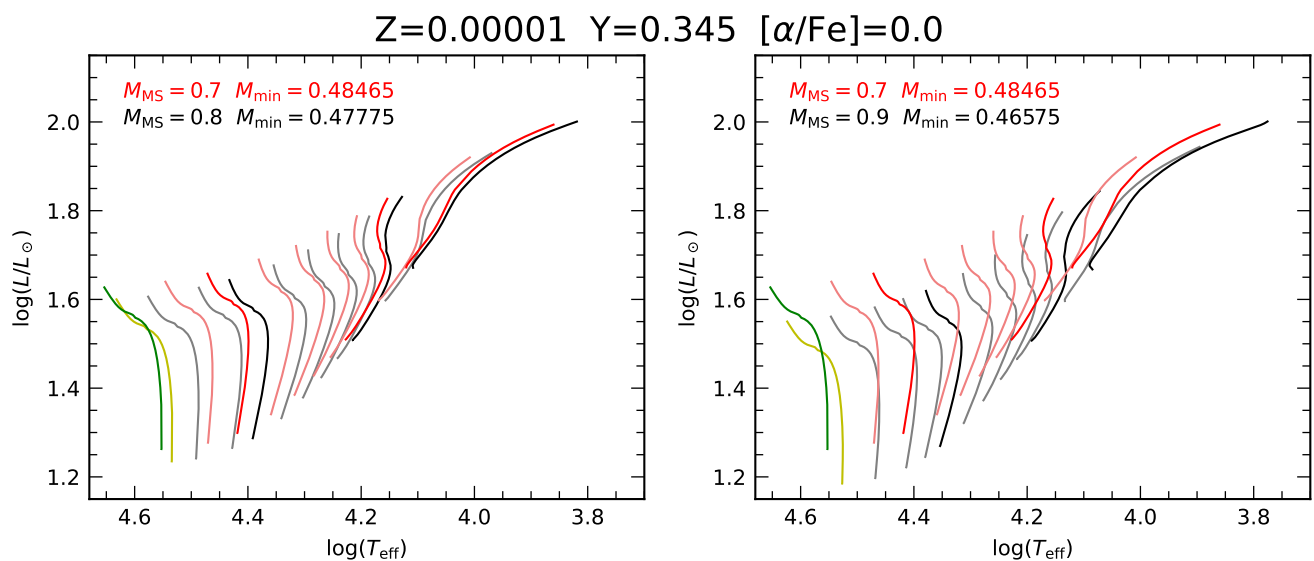
Continued on next page

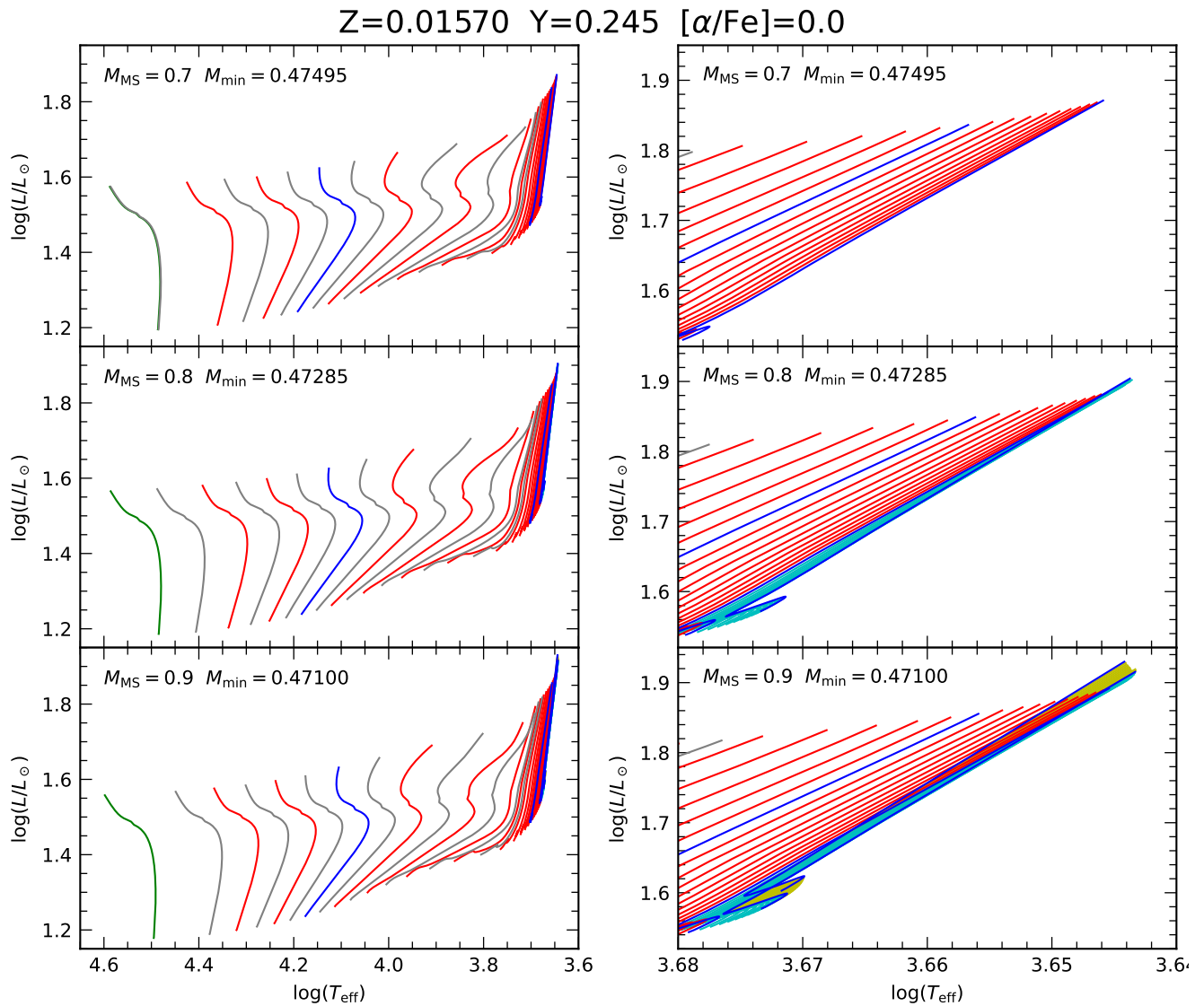
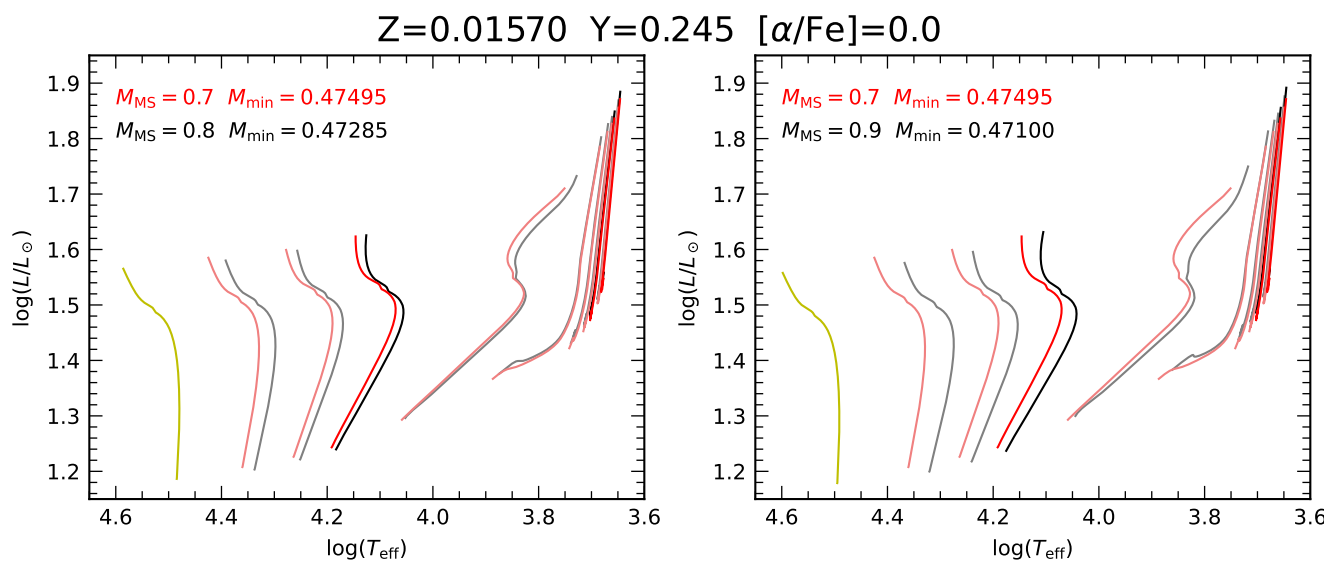
Table B.1: Continued.

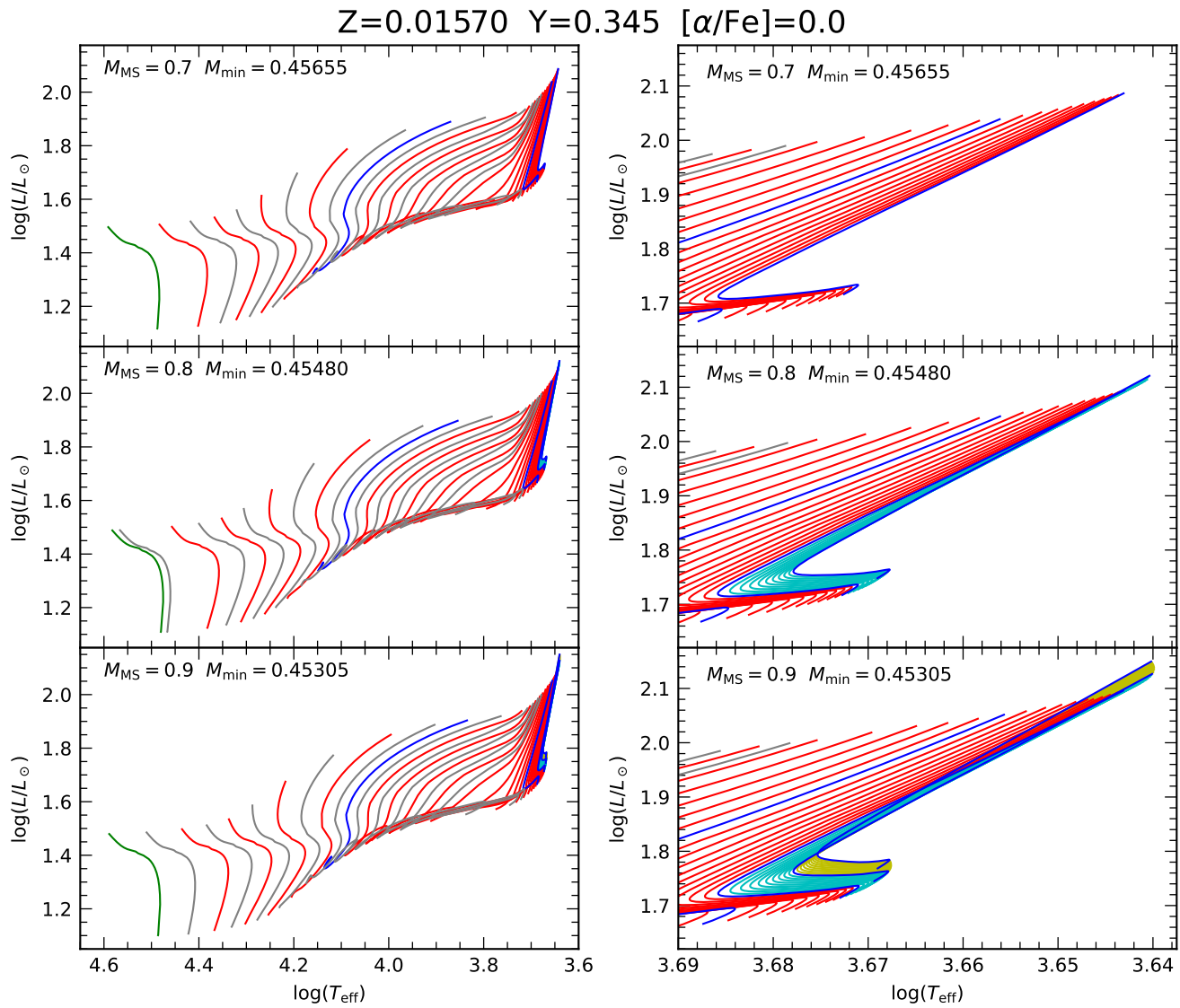
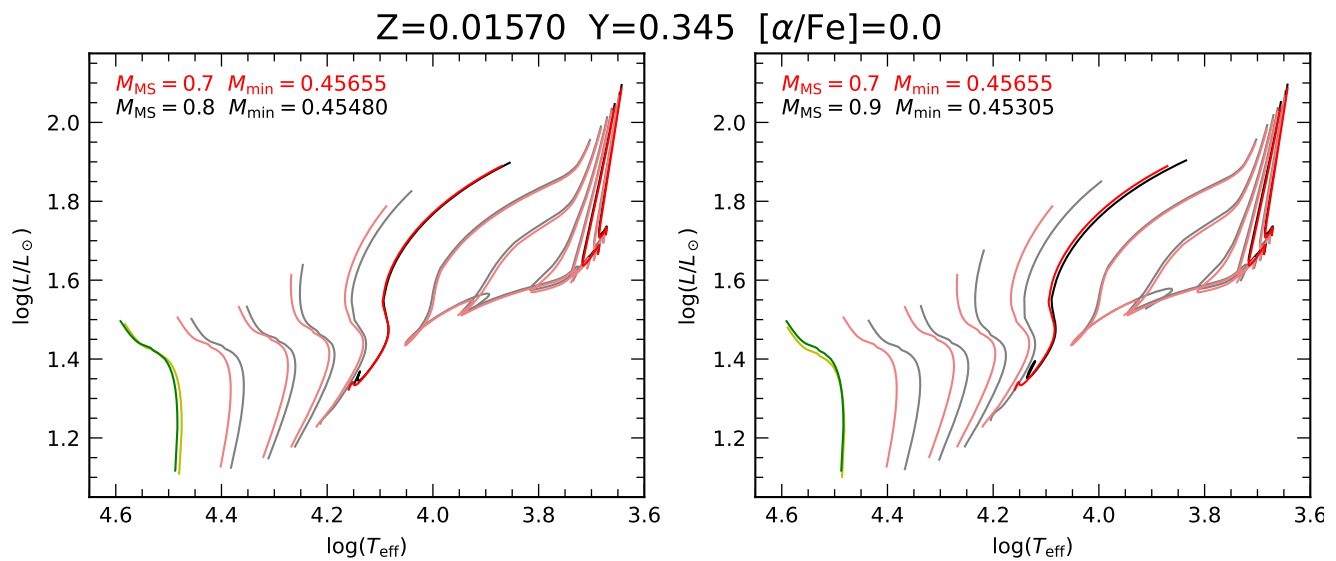
Y	M_{MS} (M_{\odot})	M_{cHe} (M_{\odot})	ΔY_{RGB}	Age (Myr)	$\log L_{3.83}^{\text{RRL}}$	$M_{3.83}^{\text{RRL}}$ (M_{\odot})	Y	M_{MS} (M_{\odot})	M_{cHe} (M_{\odot})	ΔY_{RGB}	Age (Myr)	$\log L_{3.83}^{\text{RRL}}$	$M_{3.83}^{\text{RRL}}$ (M_{\odot})
	0.800	0.4578	0.0164	30585	1.375	0.519		0.800	0.4578	0.0164	30159	1.392	0.522
	0.900	0.4563	0.0200	19809	1.376	0.517		0.900	0.4563	0.0200	19422	1.394	0.521
0.320	0.700	0.4553	0.0109	41592	1.416	0.516	0.320	0.700	0.4553	0.0108	41142	1.434	0.519
	0.800	0.4535	0.0163	25491	1.421	0.515		0.800	0.4535	0.0162	25066	1.438	0.518
	0.900	0.4521	0.0189	16503	1.421	0.513		0.900	0.4521	0.0191	16130	1.439	0.517
0.345	0.700	0.4510	0.0115	34534	1.468	0.512	0.345	0.700	0.4510	0.0115	34066	1.488	0.515
	0.800	0.4493	0.0158	21162	1.470	0.511		0.800	0.4493	0.0157	20746	1.490	0.513
	0.900	0.4479	0.0178	13694	1.470	0.509		0.900	0.4479	0.0179	13335	1.489	0.512
0.370	0.700	0.4467	0.0117	28544	1.522	0.507	0.370	0.700	0.4467	0.0117	28078	1.544	0.510
	0.800	0.4450	0.0150	17495	1.523	0.506		0.800	0.4450	0.0151	17093	1.542	0.508
	0.900	0.4437	0.0164	11311	1.522	0.504		0.900	0.4436	0.0165	10971	1.543	0.507

Appendix C: Supplementary HB track figures

To complement the example presented in Figs. 1 and 2, the figures in this appendix display three additional sets of computed HB tracks for different chemical compositions and the three M_{MS} values. Each set includes, similar to Fig. 2, a comparison between HB tracks with $M_{\text{MS}} = 0.800$ and $0.900 M_{\odot}$ against $0.700 M_{\odot}$ for the corresponding chemical composition. Specifically, Figs. C.1 and C.2 correspond to the $Z = 0.00001$, $Y = 0.345$, and $[\alpha/\text{Fe}] = 0.0$ case; Figs. C.3 and C.4, to the $Z = 0.01570$, $Y = 0.245$, and $[\alpha/\text{Fe}] = 0.0$ case; and Figs. C.5 and C.6, to the $Z = 0.01570$, $Y = 0.345$, and $[\alpha/\text{Fe}] = 0.0$ combination.


 Fig. C.1: Same as Fig. 1 but for $Y = 0.345$.

 Fig. C.2: Same as Fig. 2 but for $Y = 0.345$.

Fig. C.3: Same as Fig. 1 but for $Z = 0.01570$ and $Y = 0.245$.Fig. C.4: Same as Fig. 2 but for $Z = 0.01570$ and $Y = 0.245$.


 Fig. C.5: Same as Fig. 1 but for $Z = 0.01570$ and $Y = 0.345$.

 Fig. C.6: Same as Fig. 2 but for $Z = 0.01570$ and $Y = 0.345$.